INL/EXT-21-64101-Revision-0



# As-Run Physics Analysis for the EPRI Zirconium Growth C Capsule

August 2021

Micah D Gale

Changing the World's Energy Future

Idaho National Laboratory

*INL is a U.S. Department of Energy National Laboratory operated by Battelle Energy Alliance, LLC*

INL/EXT-21-64101-Revision-0

# As-Run Physics Analysis for the EPRI Zirconium Growth C Capsule

**Micah D Gale**

**August 2021**

**Idaho National Laboratory**
**Idaho Falls, Idaho 83415**

**http://www.inl.gov**

**Prepared for the**
**U.S. Department of Energy**
**Under DOE Idaho Operations Office**
**Contract DE-AC07-05ID14517, DE-AC07-05ID14517**

| | | | |
|---|---|---|---|
| 1. | Effective Date | 23 August 2021 | **Professional Engineer's stamp** |
| 2. | Does this ECAR involve a safety SSC? | Yes | Not required.<br>None of the criteria listed in LWP-10010 § 4.1 apply. |
| 3. | Safety SSC Determinaton Document ID | ECAR-2294 | |
| 4. | SSC ID | — | |
| 5. | Project No. | — | |
| 6. | Engineering Job (EJ) No. | — | |
| 7. | Building | — | |
| 8. | Site Area | — | |

9. Objective / Purpose

This engineering calculation and analysis report documents the as-run nuclear-heating term, source-term, and radiation damage (measured in displacements per atom [dpa]) accumulation for the Electric Power Research Institute zirconium growth experiment's C capsule (EPRI-ZG-C). These data have been calculated using MCNP 6.1 and SCALE 6.2.3. These data can be used for: the shipping of the EPRI-ZG-C capsule, the acceptance of the capsule at the Materials and Fuels Complex, and programmatic scientific needs.

10. If revision, please state the reason and list sections and/or page being affected.

A change to the data needed by HFEF was made to include data for the entire shipped capsule. While preparing these updated data it was discovered that the material definition for 304 stainless steels did not include nickel, and that more components of the capsule were activated than would actually ship. These problems have been corrected. This affected the attachments: `ShippingData.xlsx`, and `MFCdata.xlsx`. Section 5.2 was clarified in regards to the location of supporting data. Section 5.2.3 was changed to explain the new data being included. Table 2 was revised with new data requirements. It was found that the radiation damage, and the nuclear heating results for while the reactor was operated were not significantly affected. The decay heating results for the capsule actually decreased due to removing excess steel from the model.

11. Conclusion / Recommendations

In this report the radioactive source term, radioactive heating term, nuclear heating term, and radiation damage accumulation data for the EPRI-ZG-C experiment capsule were calculated. These data are available in Section 5.2, and the attached Office Open XML workbook files (.xlsx files). These data may be used for shipping of the EPRI-ZG-C capsule, accepting the EPRI-ZG-C capsule at the Materials and Fuels Complex and for furtherance of the program's scientific goals.

# Contents

**INTRODUCTION** **5**

**1 EXPERIMENT DESCRIPTION AND SCOPE OF ECAR** **5**

**2 DESIGN OR TECHNICAL PARAMETER INPUT AND SOURCES** **8**
2.1 MATERIAL COMPOSITIONS AND PROPERTIES . . . . . 8
2.2 GEOMETRY . . . . . 10
2.3 OPERATIONS DATA . . . . . 10
2.4 NUCLEAR DATA . . . . . 11

**3 ASSUMPTIONS** **12**

**4 COMPUTER CODE VALIDATION** **14**

**5 DISCUSSION/ANALYSIS** **14**
5.1 METHODS . . . . . 14
5.1.1 MATERIAL ACTIVATION . . . . . 17
5.1.2 MODEL DESCRIPTION . . . . . 18
5.1.3 CALCULATING FLUX AND NORMALIZING TALLIES . . . . . 19
5.1.4 RADIATION DAMAGE AND NICKEL . . . . . 20
5.1.5 RADIATION DAMAGE AND PROPRIETARY ALLOYS . . . . . 20
5.1.6 CALCULATING NU-BAR . . . . . 22
5.2 RESULTS . . . . . 24
5.2.1 NUCLEAR HEATING . . . . . 24
5.2.2 RADIATION DAMAGE . . . . . 24
5.2.3 ACTIVATION . . . . . 25

**6 REFERENCES** **30**

**APPENDICES** **34**

**A SIMPLIFIED IRRADIATION HISTORY FOR EPRI-ZG-C** **34**

## List of Figures

1 ATR core cross section showing experiment positions in green. . . . . 6
2 The damage-energy-cross sections for various alloy constituents of zircalloy. . . . . 21
3 A geometry plot with cell numbers from MCNP of the top of the capsule. . . . . 27
4 A geometry plot with cell numbers from MCNP of the bottom of the capsule on the X-Z plane. 28
5 A geometry plot with cell numbers from MCNP of the bottom of the capsule on the Y-Z plane. 29

## List of Tables

2 Follow-on working this ECAR as an input. [9] . . . . . 7
3 Cooldown times modeled from end of irradiation (EOI), which was October 29, 2020. . . . . 7
4 Core loading history relevant to the EPRI-ZG-C capsule. . . . . 7
5 EPRI Zircalloy Compositions Ranges [wt%]. . . . . 8
6 Hydrogen content in zircalloy samples [1]. . . . . 9
7 Material Densities used for modeling. . . . . 9
8 INL design drawings relevant to these experiments. . . . . 10
9 A summary of the core and total power for cycles of interest. . . . . 11
10 Thermal neutron-molecular interaction, $s(\alpha, \beta)$, data used for modeling materials. . . . . 11
11 Software used for this analysis. . . . . 14
12 Hardware used for this analysis. . . . . 14
13 The git SHA-1 hashes of the commits for scripts used in this ECAR. . . . . 16
14 ***Example*** data to be given for radiation damage for showing calculation process. . . . . 22
15 Constants and input data used for flux normalization. . . . . 22
16 Normalization factors used for various tallies. . . . . 23
17 The uncorrected radiation damage by constituent element. . . . . 25
18 Data needed for implementing the nickel correction factor for radiation damage [46][47]. . 25
19 Extreme possible values for sample radiation damage accumulation . . . . . 25
20 The irradiation history for EPRI-ZG-C simplified into constant-power sections. . . . . 34
20 (continued). . . . . 35
20 (continued). . . . . 36
20 (continued). . . . . 37

# PROJECT ROLES AND RESPONSIBILITIES

| Project Role | Name | Organization | Pages Covered (if applicable) |
|---|---|---|---|
| Performer | Micah D. Gale | C150 | — |
| Checker[a] | Jill R. Mitchell | C150 | Sections 1 – 5.2 except 5.1.1 and 5.2.3 |
| | Connie M. Hill | C150 | Sections 5.1.1, 5.2.3 and supporting documents: 'shippingData.xlsx' and 'MFCdata.xlsx' |
| Independent Reviwer[b] | Dong O. Choe | C150 | — |
| CUI Reviewer[c] | See LRS: INL/EXT-21-64101 | — | — |
| Manager[d] | Joshua L. Peterson-Droogh | C150 | — |
| Requestor[ef] | Matthew M. Arrowood | C640 | — |
| Experiment Safety Analysis Author[f] | Stephen Evans | G520 | — |
| Document Owner[f] | Boopathy Kombaiah | U520 | — |
| Reviewer[f] | — | — | — |

**Responsiblities:**

a. Confirmation of completeness, mathematical accuracy, and correctness of data and appropriateness of assumptions.

b. Concurrence of method or approach. See definition, LWP-10106.

c. Concurrence with the document's markings in accordance with LWP-11202.

d. Concurrence of procedure compliance. Concurrence with method/approach and conclusion.

e. Authorizes the commencement of work of the engineering deliverable. See Appendix A.

f. Concurrence with the document's assumptions and input information. See definition of Acceptance, LWP-10200.

**NOTE:** *Delete or mark "N/A" for project roles not engaged. Include ALL personnel and their roles listed above in the eCR system. The list of the roles above is not all inclusive. If needed, the list can be extended or reduced.*

# INTRODUCTION

This Engineering Calculation and Analysis Report (ECAR) documents the as-run neutronics modeling of the C capsule of the Zirconium Growth experiment from the Electric Power Research Insitute (EPRI). This experiment is referred to as EPRI-ZG, and the capsule is referred to as EPRI-ZG-C. The capsule was loaded in the Advanced Test Reactor (ATR) intermittently between cycles 149B and 168B. During these irradiations, the capsule was loaded in A14 (near the SE lobe) and A15 (Near the SW lobe). See Figure 1 for an ATR core map.

This analysis covers:

- The nuclear heating (gamma and neutron) rates for the experimental capsule during irradiation.
- The radiation damage (measured in displacements per atom [dpa]) accumulated for the experiments.
- The radioactivity and the decay heat term of the materials from activation.

# 1 EXPERIMENT DESCRIPTION AND SCOPE OF ECAR

A capsule in the EPRI-ZG experiment consists of 50 zirconium alloy (zircalloy) specimens held in position with a type 304L stainless-steel sample holder and encapsulated in a type 304L stainless-steel capsule. The EPRI-ZG-C capsule was irradiated to approximately 20 dpa. An insulator disc made of zirconia separated the specimens and holder from the bottom of the capsule to aid in temperature control. Disc springs between the top of the holder and the top of the capsule held the holder and specimens in place. The rows of specimens were separated by zircalloy spacers. A gas gap between the holder and the interior capsule wall provided the means of achieving the desired temperature. The gas gap contained helium to maintain the desired temperature at the designated ATR lobe power. The gas mixture did not flow and therefore required the lobe power to be constant to maintain the desired temperature. The capsule was designed to connect to an upper and lower type 304L basket piece to center the capsule vertically in the ATR core [1].

The specimens are arranged in the capsule in 10 rows of 5 columns for a total of 50 specimens. The top and bottom rows of specimens (Row 10 and Row 1, respectively) are sacrificial buffer specimens used to maintain temperature uniformity over the remaining 40 specimens. Each of the remaining 40 specimens were made of proprietary zircalloy compositions, 15 of which were pre-hydrided to different levels. The composition of the specimens is shown in Table 5. All of those alloys have a proprietary composition. The compositions of the vendor proprietary samples (AG, BG, AW, BW, and AA) were kept proprietary and the composition ranges are given in Table 5. The EPRI proprietary alloys (Ar10, Ar20, Ar30, and Ar36) compositions are given in a proprietary EPRI report [2], and were explicitly modeled given these data. The nomenclature for the level of hydrogen doping in a sample is presented in Table 6. The specimens are numbered with the row number followed by the column number separated by a hyphen (e.g., the specimen in Row 3 Column 2 will be specimen number 3-2). The capsule was inserted into the outboard A positions A14 and A15. The exact capsule loading by alloy type is provided in Table 4 of the Irradiation Test Plan [1]. Figure 1 shows the core map of ATR.

The experiment in the nearest position (i.e., A10 or A11) was most commonly an Advanced Fuels Campaign (AFC) experiment. All of these experiments consisted of a fuel specimen inside of a cadmium basket. The cadmium was replaced every cycle [4]. For one cycle a solid flow restrictor—outboard position (SFROP), which is an aluminum-6061 dummy rod [5], was inserted in the adjacent position [6]. For another cycle, the AFC experiment was replaced with an HSA cobalt assembly [7]. Table 4 provides the details on the core loading histories relevant to EPRI-ZG-C.

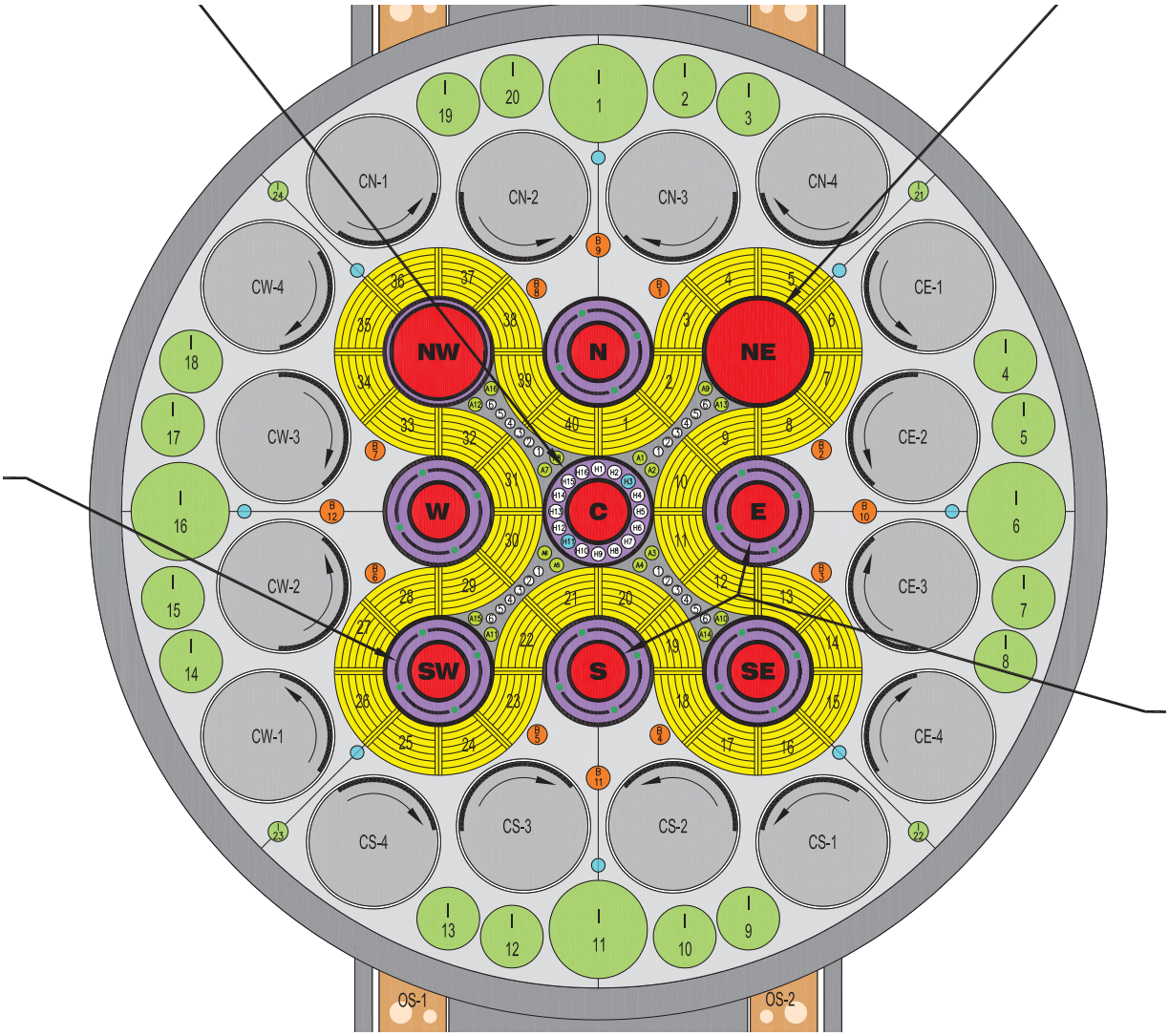


Figure 1: ATR core cross section showing experiment positions in green. Positions A14 and A15 are in the neck-shim housing inside of the fuel elements near the SE and SW flux traps, respectively [3].

This ECAR supports programmatic needs, and the safety basis for shipping from ATR to MFC and for MFC operations. The program needs the as-run nuclear heating terms during irradiation for the experiment as well as the radiation damage [dpa] accumulation of the samples. To support the safety analysis for shipping and MFC operations, a radioactive source term is needed. To support the shipping safety analysis the decay heating source term is needed as well. These requirements are specified in more detail in Table 2. From these, we determined which cooldown periods would be calculated, and these are given in Table 3. For reference, the irradiation ended with Cycle 168B on October 29, 2020 [8].

Table 2: Follow-on working this ECAR as an input. [9]

| | **Follow-on Requirement** | | |
|---|---|---|---|
| | **Thermal-Hydraulics As-Run** | **Shipping** | **MFC HFEF Acceptance** |
| Data Type | Nuclear heating | Decay heating, source term | Source term |
| Units | $\frac{W}{g}$ | $\frac{W}{g}$, Ci | g |
| Timing | During irradiation | Just prior to BEA Research Reactor (BRR) cask loading | Just prior to cask unloading |
| Minimum Threshold | — | $10^{-11}$ | $10^{-10}$ |
| Granularity | Sample | Assembly | Sample & assembly |
| File Format | Office Open XML workbook (.xlsx) | .xlsx | .xlsx |

Table 3: Cooldown times modeled from end of irradiation (EOI), which was October 29, 2020.

| **Time since EOI [d]** | **Date** |
|---|---|
| 120 | Feb 26, 2021 |
| 180 | April 27, 2021 |
| 210 | May 27, 2021 |
| 280 | Aug 5, 2021 |

Table 4: Core loading history relevant to the EPRI-ZG-C capsule.

| **Cycle** | **SE Lobe** | | **SW Lobe** | |
|---|---|---|---|---|
| | **A10** | **A14** | **A11** | **A15** |
| 149B [7] | | | HSA Cobalt | EPRI-ZG-C |
| 150B [10] | | | AFC-3B | EPRI-ZG-C |
| 151A [11] | | | AFC-3B | EPRI-ZG-C |
| 151B [12] | | | AFC-3B | EPRI-ZG-C |
| 152B [6] | | | SFROP | EPRI-ZG-C |
| 155B [13] | AFC-3C | EPRI-ZG-C | | |
| 158B [14] | AFC-4C | EPRI-ZG-C | | |
| 160B [15] | | | AFC-3F | EPRI-ZG-C |
| 162B [16] | AFC-4C | EPRI-ZG-C | | |
| 164A [17] | | | AFC-3F | EPRI-ZG-C |
| 164B [18] | | | AFC-3F | EPRI-ZG-C |
| 168A [19] | AFC-4B | EPRI-ZG-C | | |
| 168B [20] | | | AFC-3F | EPRI-ZG-C |

# 2 DESIGN OR TECHNICAL PARAMETER INPUT AND SOURCES

## 2.1 MATERIAL COMPOSITIONS AND PROPERTIES

All sample material compositions are provided by the program via PLN-3303[1], or the EPRI proprietary report [2]. For convenience, some of these data are presented here in Tables 5 & 6. Samples composed of the alloys: AG, BG, AW, BW, and AA are described in PLN-3303, and only a broad range are given for these compositions. For alloys Ar10, Ar20, and Ar36 the compositions are provided in the EPRI report. Other structural materials are used in manufacturing the capsule, including:

- aluminum 6061-T6 [21]
- 304L stainless steel in bar [22] and rod [23] forms
- Nitronic 60 stainless steel [24]
- Zirconia ($ZrO_2$)
- Silica quartz ($SiO_2$)
- Silicon carbide (SiC)
- Various melt wires of varying compositions of:
  - Sn
  - Sb
  - Pb
  - Au
  - Ag

Table 5: EPRI Zircalloy Compositions Ranges [wt%].

| **Element** | **AG** [1] | **BG** [1] | **AW** [1] | **BW** [1] | **AA** [1] |
|---|---|---|---|---|---|
| tin | 0–1.2 | | | | |
| niobium | 0–1.2 | | | | |
| iron | 0–1.2 | | | | |
| chromium | 0–0.1 | | | | |
| nickel | 0–0.1 | | | | |
| vanadium | 0–0.1 | | | | |
| oxygen | 0–0.2 | | | | |
| hydrogen | 0–0.1 | | | | |
| zirconium | >97[1] | | | | |

1. Alloys AG–AA are vendor proprietary alloys with compositions within the limits indicated. The sum of the total alloying additions is <3 wt.%. The remaining balance of the material, >97 wt.%, is zirconium.

The compositions of these alloys are provided in their respective ASTM standards as cited. These citations were taken directly from the relevant drawings. In cases where alloying additives (e.g., Ni in steel) were specified as a range, the maximum allowable value for the range was used for modeling.

Table 6: Hydrogen content in zircalloy samples [1].

| Hydrogen Content Description | Hydrogen Content [wt-ppm] | Designation |
|---|---|---|
| Zr in as-recieved condition | 0 | x |
| Hydrogen content at solubility limit in Zr | 40 | y |
| Hydrogen content above solubility limit in Zr | 125 | z |

These standards do not provide information on the densities of these materials. This analysis used the densities from the relevant ASM International handbooks. The densities used are provided in Table 7. For the melt wires, some of the compositions used are atypical for a commercial alloy, and therefore data do not exist for their densities. In these cases, the densities of the pure metals were averaged weighted by composition, to form the alloy density. The density of the helium fill gas was calculated assuming a temperature of 293.15 K and a pressure of 1.0 atm.

For modeling in MCNP, we used atom densities. These were calculated based on the element's atomic weight [25], the element's naturally occurring isotopic abundance [26], and required Avogadro's number ($N_a$)[27].

Table 7: Material densities used for modeling. These densities are reported as engineering inputs, so atom densities are not listed for most materials here, as those were not provided by the references. Note that all zircalloys were treated as having the same density.

| Material | Mass Density $\left[\frac{g}{cm^3}\right]$ | Atom Density $\left[\frac{10^{24}atom}{cm^3}\right]$ |
|---|---|---|
| Zircalloy [28] | 6.57 | — |
| 304L [29] | 8.0 | — |
| 316 [29] | 8.0 | — |
| Nitronic 60[1] | 8.0 | — |
| 6061 [30] | 2.7 | — |
| Ni [31] | 8.9 | — |
| CoAl[2] [31] | 2.70 | — |
| Sn [31] | 7.298 | — |
| Sb [31] | 6.697 | — |
| Pb [31] | 11.3 | — |
| Au [31] | 19.302 | — |
| Ag [31] | 10.49 | — |
| quartz [32] | 2.65 | — |
| SiC [32] | 3.2 | — |
| Zirconia [32] | 5.8 | — |
| He gas[3] | — | 2.5034E-05 |

1. Data were not readily available for this alloy. It was assumed to have the same density as the other stainless steels.
2. Calculated as a weighted average.
3. Calculated as a gas at 1 atm and 294.15 K.

## 2.2 GEOMETRY

The geometry modeled for the capsule was based off the as-designed geometry. Nominal values for all dimensions were used. If only bilateral limits with no nominal value were given, the average of the two limits were used. The relevant drawings are listed in Table 8.

Table 8: INL design drawings relevant to these experiments.

| INL Drawing | Drawing Description |
|---|---|
| *EPRI-ZG-C* | |
| 601412 | Complete test rig Assembly |
| 601413 | Sample capsule assembly |
| 601414 | Sample capsule details |
| 601415 | Test holder assembly |
| 601416 | Test holder details |
| 601417 | Test specimens and spacers |
| 601418 | Test basket extension details |
| 602748 | Flux monitor holder |
| *SFROP* | |
| 120421 | SFROP and other flow restrictors details |
| *Cobalt* | |
| 603424 | Low specific activity (LSA) cobalt capsule assembly and details |
| 427648 | “Old” HSA cobalt capsule assembly. |

The geometry for the whole reactor core was taken from the models in ECAR-4644 [33]. The geometry for an AFC experiment was taken from the models used in ECAR-3139 [34].

The geometry for the EPRI-ZG-C capsule was created in the MCNP models for this ECAR, and was simplified in the following ways:

1. The sampler spacers were not modeled as “I-beams” but rather as right rectangular prisms. This increased the spacers’ overall volume, so the spacers’ densities were reduced accordingly in order to preserve mass.
2. Prior to shipping, the capsule will be resized, and much of the test basket will be discarded. The lower portion of this basket, which was discarded, was not modeled.
3. All fillets, chamfers, and threads were removed. No attempt to preserve total mass was made.
4. The retainer springs were not modeled.
5. The melt wire capsule was modeled as a right circular cylinder. In reality, the ends were melted shut.
6. The SFROP was modeled solely as a right circular cylinder.

## 2.3 OPERATIONS DATA

Data for the operation of ATR for the relevant cycles were retrieved from the Nuclear Data Managements and Analysis System (NDMAS) [8]. These data included the lobe and total power and the insertion of neck-shim rods. These data were downloaded from the system in an Office Open XML workbook (.xlsx), and then converted into a comma-separated values file (.csv). A summary of the relevant cycle history is provided in table 9.

Table 9: A summary of the core and total power for cycles of interest. The lobe power is only for the lobe in which EPRI-ZG-C was loaded. The Effective Nominal Power Days (ENPD) are provided as well. These are the number of days at the average power for that cycle required to release same amount of energy.

| Cycle | Lobe Power [MW] | Core Power [MW] | ENPD [d] |
|---|---|---|---|
| 149B | 22.86 | 105.26 | 53.82 |
| 150B | 22.84 | 107.06 | 41.76 |
| 151A | 22.31 | 96.06 | 59.38 |
| 151B | 22.79 | 100.6 | 51.67 |
| 152B | 22.74 | 102.32 | 51.39 |
| 155B | 22.68 | 103.37 | 50.49 |
| 158B | 22.94 | 100.96 | 51.49 |
| 160B | 22.83 | 107.39 | 60.41 |
| 162B | 22.68 | 99.04 | 38.97 |
| 164A | 21.98 | 101.25 | 55.83 |
| 164B | 22.7 | 101.66 | 63.83 |
| 168A | 22.6 | 108.98 | 62.09 |
| 168B | 23.4 | 104.91 | 56.53 |

## 2.4 NUCLEAR DATA

For delayed photon transport, all materials used photo-atomic data from the ENDF/B-VI.8 library [35]. All nuclear data for the experiment capsule used the ENDF/B-VII.1 library [36]. Specifically, the nuclear data that were Doppler broadened by the MCNP developers to 600 K were used. The remaining materials use a variety of nuclear data libraries provided in their respective ECAR's.

When possible, thermal neutron-molecular interaction, $s(\alpha, \beta)$, data were used. The data used for various materials are listed in Table 10.

Table 10: Thermal neutron-molecular interaction, $s(\alpha, \beta)$, data used for modeling materials.

| Material | $s(\alpha, \beta)$ Data Used |
|---|---|
| Homogenized fuel | H-light water |
| Homogenized reflector | H-light water, Be |
| EPRI-ZG-C stainless steel | Fe-56 |
| EPRI-ZG-C zircalloy | H-ZrH |
| EPRI-ZG-C aluminum | Al-27 |

For postprocessing of the data $\bar{\nu}$, the average number of neutrons produced by a fission and $Q$, the amount of energy released in a fission, are needed. These data were taken from ENDF/B-VII.1 for U-235, and the energy released as neutrinos was ignored.

# 3 ASSUMPTIONS

1. The melt wires are small enough to be neutron-transparent enough to not have significant resonance self-shielding. This assumption was confirmed through a scoping analysis that showed no detectable effect from the melt wires on the neutron flux. Therefore, one melt wire material will be neutronically modeled. The fluxes were used to activate all melt wire capsules. This will effectively remove resonance self-shielding, which will over-predict the reaction rates and, therefore, the material activation.

2. The Doppler broadening temperature differences between the cross section used at 327°C versus the experiment's operating temperature of 285°C is negligible. This was confirmed with scoping studies, which showed no effect on the flux from spatial self-shielding when room temperature cross sections were used. In addition, no significant effect on the radiation damage reaction rate was found either, showing that these materials are not extreme resonant absorbers and Doppler broadening effects can be ignored.

3. Though the temperature of the experiment components will vary during steady-state operations, the effects of Doppler broadening on nuclear heating are negligible.

4. The rotation of the outer shim control cylinders (OSCC's) is negligible and was modeled at a constant position. The experiment position is inside of the neck-shim housing of the ATR, on the opposite side of the driver fuel from the OSCC's. If the effect of driver fuel depletion on the experiment is negligible, the effects of OSCC's will be even less due to the distance they are from the experiment.

5. The average threshold displacement energy, $E_D$, for calculating radiation damage is 40 eV for all metals. This is done to maintain consistency with previous ECARs for this project.

6. All elements in the zircalloys have nearly equal atomic weights, and these impurities have no affect on the crystal lattice of the zirconium. Therefore, radiation damage contributions can be simply a weighted sum for all constituents.

7. The only isotope that fissions in the driver fuel is U-235. Since the driver fuel is highly enriched uranium (HEU), Plutonium production is negligible.

8. Driver fuel burnup is negligible. The HEU does not significantly change its neutron source spectrum with burn-up, due to it not breeding significant amounts of plutonium or other actinides. The main effect of driver fuel depletion is the burnup of the fuel near the core center-line, leading to a flattened flux distribution. The sample capsule is around 16 inches long, and when compared to the active core height of 48 inches, this flux flattening has little effect on the samples. This was confirmed with a scoping analysis.

9. The fuel, but not the cadmium basket, in the nearby AFC-fueled experiments is negligible. This has been confirmed with a scoping analysis.

10. The fuel in flux trap experiments is negligible. This has been confirmed with a scoping analysis.

11. The effect of HSA cobalt assembly is comparable to that of a SFROP. This was confirmed with a scoping analysis for a LSA cobalt assembly. The LSA cobalt assembly's effect was closer to that of the SFROP's than that of the AFC cadmium basket. The HSA assembly contains less cobalt than the LSA assembly; therefore, it is more neutron transparent and more similar to a SFROP.

12. A neck-shim rod in regulating rod mode, where it is driven by the control computer, is assumed to be the same as a fully removed rod. The only neck-shim rod used as regulating rod is the fourth rod [3], which is close enough to the capsule to have an effect on the experiment. The regulating rod's tip is usually maintained near the core center-line. This is a conservative assumption.

13. The nearest neck-shim to the capsule which is fully inserted, will have the largest impact on the capsule. The models had all neck-shims behind the closest insert rod also inserted. For example, if only Neck-shims 4,5, and 6 were inserted in the lobe during a cycle, this would be modeled as all neck-shims in that lobe being inserted.

14. Following the rules above: Neck-shim #1 being inserted is comparable to no neck-shim rods being inserted, and Neck-shim #2, #3 or, #4 are all comparable to Neck-shim #3 being inserted. This means the only scenarios modeled had 0, 3, 5, or 6 neck-shim rods inserted. Rods were sequentially inserted in the model from the core center moving out towards the flux trap.

15. All relevant core loading can be modeled in the southwest lobe, even though the experiment was frequently in the southeast lobe. The only differences between these lobes are the experiments loaded, the neck-shim rods inserted, the driver fuel composition, and the lobe power. All of these differences have either been found to be negligible, or are being explicitly modeled.

16. All other experiments in the ATR were negligible.

17. Rotation of the experiment relative to the driver fuel is neglected. The experiment is so neutron transparent that no appreciable flux gradient forms necessitating tracking the rotation.

18. None of the materials have impurities. All materials were modeled with the compositions provided in the relevant citations.

19. The density of Nitronic 60 stainless steel has the same mass density as 304L and 316 stainless steels.

20. In the INL design drawings when nominal values were not given, but only bilateral tolerances, the average of the tolerances were assumed to be the nominal values for geometry modeling.

Table 11: Software used for this analysis.

| Software Package | Version | EA indentifier (UUID) | V&V plan |
|---|---|---|---|
| MCNP6 | release 1.0 | 07B1DA62-52CC-4A40-A632-6327D4AB4519 | TEV-2944[37] |
| SCALE 6 | release 2.3 | 1DDD52F4-43ED-4744-95C3-A5FDB4789C58 | TEV-3686[38] |

Table 12: Hardware used for this analysis.

| Computer | Hardware | Operating System |
|---|---|---|
| Lemhi (Dell PowerEdge distributed memory system) | • 504 Compute Nodes:<br>– 2 Intel Gold 6148 CPUs (40 cores total)<br>– 192 GB RAM<br>• 2 Login Nodes:<br>– 2 Intel Gold 6148 CPUs (40 cores total)<br>– 384 GB RAM<br>• OmniPath Interconnect | CentOS 7.6 |

# 4 COMPUTER CODE VALIDATION

The modeling was performed using Monte Carlo N-Particle (MCNP) 6.1, and SCALE 6.2.3. These software are qualified for scientific and engineering use, as is documented in INL's Enterprise Architecture system. These software are further described in Table 11. As cited in Table 11, both software have been verified and validated (V&V), on two of INL's high performance computing (HPC) clusters: Falcon and Lemhi. Table 12 lists the configurations of the computing systems on which these software were run. MCNP and SCALE runs used for this ECAR were exclusively run on Lemhi.

# 5 DISCUSSION/ANALYSIS

## 5.1 METHODS

Particle transport (neutron and photon) was performed in the Monte Carlo N-Particle (MCNP) transport code [39]. The output of which was fine multigroup flux data. These data were then used to complete activation and decay analyses in the SCALE code suite, specifically in the Oak Ridge Isotope Generation (ORIGEN) and COUPLE modules [40].

Automation via the python scripting language [41] was employed in many steps of this process. Python was used to take the material composition data given in Section 2.1 and then calculate the isotopic composition of the experiments' materials, in order to create material definitions for the MCNP model. Python was then used to combine the fragmented input files to create many MCNP input files for the various scenarios modeled. For more details on the scenarios modeled, see Section 5.1.2.

For retrieving tally data from the outputs for scoping and nonactivation purposes, python was used along with the mcnptools library [42].

The MCNP ORIGEN Activation Automator (MOAA) coupled MCNP with SCALE. This tool is written in python and is meant to automatically:

- Prepare the MCNP inputs for the data needed by the COUPLE module. These data include the flux spectrum and reaction rates for reactions of interest.
- Parse the outputs from the MCNP run and use that data to create an activation library via COUPLE.
- Conduct the activation and decay of the cells of interest in the MCNP module using provided information about reactor operation.

This is accomplished through the following process:

- The user specifies parameters for MOAA through a text-based data file.
- MOAA is run on the MCNP input file prior to the official MCNP run. A tally is specified to: measure the flux spectrum in SCALE's 252-group structure and the reaction rate for the nuclear reactions of interest. For the reactions of interest, the activation library's reaction rate is replaced by the one calculated by MCNP. For all other reactions, the flux and the default SCALE nuclear data are used to calculate a reaction rate. Supporting material specifications are added to calculate the reaction rates in MCNP. The original MCNP input is not modified, but copied, and the above are appended to it.
- The user runs the new input file in MCNP (likely on the HPC).
- MOAA is run again on the output. MOAA extracts the data from the tally it specified. It then uses these data to create a COUPLE and ORIGEN run for every cell of interest. These data are then parsed and saved to a CSV file.

However, by default, MOAA performs a single constant-power irradiation followed by a cooldown period. This is not sufficient for the complex loading history that EPRI-ZG-C has had. Therefore, MOAA was modified to handle more complex irradiations.

First, a python script was created to read, and then simplify, EPRI-ZG-C's loading and reactor operations history. The loading data are from Table 4, and the operations data were retrieved from NDMAS [8]. The daily average values were used for the operating history. First, the power history was converted into a piece-wise functions of constant-power steps (e.g., 10.5 days at 23 MW, 2.5 days at 10 MW). A new constant-power step was started when the daily-average power changed by more than 9% (approximately the uncertainty in core power data). During the constant-power step, the power was averaged. Outages, or SCRAMs were added as zero-power steps. Next, changes in core configurations were added. This was based on what was loaded in the adjacent experiment position (i.e., A10 or A11) or the neck-shim rod configuration in the relevant lobe. The assumptions relevant to neck-shim configuration were factored in prior to this simplification. This simplified the irradiation history into 101 distinct steps. These are provided in Appendix A.

Only a single whole reactor core model was used. However, between cycles, the "core-split" was often changed, shifting power between the lobes. Since the whole core was modeled, all fluxes are normalized to the whole core power. Therefore, a power correction factor is needed to achieve the desired lobe power by adjusting the whole core power based on the different "core-splits." This correction factor was based on:

$$C_{p,c} = \frac{\frac{P_{l,c}}{P_{T,c}}}{\frac{P_{l,m}}{P_{T,m}}} \tag{1}$$

where

- $C_{p,c}$ is the power correction factor, which the cycle's whole core power is multiplied by,
- $P_l$ is the lobe power,
- $P_T$ is the whole core power,
- the $c$ index is for the powers of the cycle to be corrected,
- and the $m$ index is for the powers of the model used in MCNP.

To find the modeled powers in each MCNP run the fission heating "F7" tally data were used. The ratio of all power generated by driver fuel regions in a lobe were divided by the total power produced by all fuel regions. It was found that due to the changing neck-shim rod configurations the modeled "core-splits" were highly variant. MOAA only supports using a single modeled power-split, so this feature was not used, and the power was manually corrected in Microsoft Excel.

The tool MOAA was then modified to work with this irradiation history. The simplified irradiation history was provided to it in a csv file. MOAA then used a regular expression to first find the relevant MCNP input files, and then match it to the corresponding core configuration in the irradiation history. COUPLE was run for each core configuration with the relevant multi-group flux spectrum and reaction rate data calculated by MCNP as inputs, saving the outputs to separate activation libraries (f33 files). A series of ORIGEN cases were then built with the required power history. A new case was created each time the core configuration changed. MOAA also "flattened" the flux. This was done while calculating the flux for each cell. The maximum scalar flux value for any cell was taken and applied to all other cells.

The python scripts used, including MOAA were not compliant with Nuclear Quality Assurance-1 standard. Due to this, as part of the checking process for this ECAR all inputs and outputs of these scripts were checked to ensure the calculations were performed properly. The SCALE modules COUPLE and ORIGEN were only ran on the HPC Lemhi for this ECAR.

The git secure hashing algorithm (SHA)-1 hash for the versions of custom scripts used are available in Table 13.

Table 13: The git SHA-1 hashes of the commits for scripts used in this ECAR.

| **Script** | **Use** | **git SHA-1** | **URL** |
|---|---|---|---|
| generateInputs.py | Splices input files together, creates PBS runner scripts | d5002a55 | gitlab:epri-zg-c |
| MOAA | Performs activation in ORIGEN using MCNP output data | edd5c83 | gitlab:moaa |
| parseIrradiationHistory.py | Parses cycle and loading data to generate a simplified irradiation history. | 5c833ae3 | gitlab:epri-zg-c |
| parseOutputs.py | Parses MCNP mctal output tally files and MOAA outputs and stores these data in workbooks. | 3e179145 | gitlab:epri-zg-c |
| analysis_tools | Generates MCNP material definitions. Parsed mctal file as an mcnptools wrapper. | 60312329 | gitlab:analysis_tools |

### 5.1.1 MATERIAL ACTIVATION

The MCNP ORIGEN Activation Automator (MOAA) coupled MCNP with SCALE. This tool is written in python and is meant to automatically:

- Prepare the MCNP inputs for the data needed by the COUPLE module. These data include the flux spectrum and reaction rates for reactions of interest.
- Parse the outputs from the MCNP run and use that data to create an activation library via COUPLE.
- Conduct the activation and decay of the cells of interest in the MCNP module using provided information about reactor operation.

This is accomplished through the following process:

- The user specifies parameters for MOAA through a text-based data file.
- MOAA is run on the MCNP input file prior to the official MCNP run. A tally is specified to: measure the flux spectrum in SCALE's 252-group structure and the reaction rate for the nuclear reactions of interest. For the reactions of interest, the activation library's reaction rate is replaced by the one calculated by MCNP. For all other reactions, the flux and the default SCALE nuclear data are used to calculate a reaction rate. Supporting material specifications are added to calculate the reaction rates in MCNP. The original MCNP input is not modified, but copied, and the above are appended to it.
- The user runs the new input file in MCNP (likely on the HPC).
- MOAA is run again on the output. MOAA extracts the data from the tally it specified. It then uses these data to create a COUPLE and ORIGEN run for every cell of interest. These data are then parsed and saved to a CSV file.

However, by default, MOAA performs a single constant-power irradiation followed by a cooldown period. This is not sufficient for the complex loading history that EPRI-ZG-C has had. Therefore, MOAA was modified to handle more complex irradiations.

First, a python script was created to read, and then simplify, EPRI-ZG-C's loading and reactor operations history. The loading data are from Table 4, and the operations data were retrieved from NDMAS [8]. The daily average values were used for the operating history. First, the power history was converted into a piece-wise functions of constant-power steps (e.g., 10.5 days at 23 MW, 2.5 days at 10 MW). A new constant-power step was started when the daily-average power changed by more than 9% (approximately the uncertainty in core power data). During the constant-power step, the power was averaged. Outages, or SCRAMs were added as zero-power steps. Next, changes in core configurations were added. This was based on what was loaded in the adjacent experiment position (i.e., A10 or A11) or the neck-shim rod configuration in the relevant lobe. The assumptions relevant to neck-shim configuration were factored in prior to this simplification. This simplified the irradiation history into 101 distinct steps. These are provided in Appendix A.

The reactions of interest were chosen for this specific experiment. A simple test run was completed in ORIGEN to activate all elements involved in the problem for 10 years in a flux for this position based on previous modeling. This was then used to find all isotopes that could be involved in the problem based on SCALE's nuclear data. All of these nuclides were listed as isotopes of interest, if they are included in the ENDF/B-VII.1 library. The reactions of interest included were the $(n, \gamma)$, $(n, p)$, and $(n, \alpha)$ reactions. Fission was not included as this was a structural material irradiation. Note that these are not the only

reactions that were considered by ORIGEN. For these reactions the reaction rates were calculated by MCNP at the correct temperature. For all other reactions that ORIGEN considered the reaction rate was calculated at the SCALE nuclear data default temperature.

The melt wire capsules were modeled slightly differently from the rest of the materials. For simplicity only one melt-wire capsule type was modeled in the MCNP model. This was a capsule with two pure tin wires.

The melt-wire capsule was modeled as if it was a hollow right-circular cylinder. In reality the ends were melted shut from this starting cylindrical shape. This led to the model having excess glass material to form the top and bottom walls. This is a conservative assumption as the excess material will lead to a higher radioactivity than the actual melt wire vial has in reality.

For modeling the activation of the actual melt wires the measured fluxes in MCNP for the modeled melt wire was used. Separate activation cases were ran for each melt wire constituent element. These data were then multiplied by each melt-wire composition and the melt wire mass, to find the isotopics for each melt-wire type. These data are never directly reported. For the MFC report the isotopics are combined with that of the glass vials. These data are then compared and the maximum value for each isotope is taken, over-predicting the radioactivity for any given melt-wire capsule.

### 5.1.2 MODEL DESCRIPTION

The model of the EPRI-ZG-C capsule was built in MCNP by the performer. The model was based on the geometry described in Section 2.2, with the simplifications mentioned and nominal dimensional values. The materials used were based on Section 2.1, and each samples' material composition was explicitly modeled. The performer of this ECAR also created a simplified SFROP model.

The nuclear data were taken from the libraries given in Section 2.4. For the nuclear data, the data were Doppler broadened to 600 K (i.e., the 71c MCNP data). The photoatomic data have no temperature dependence.

For each core configuration modeled, two transports with different transport modes were performed. The first was intended to complete the neutron transport as well as provide the prompt heating data. For this first mode, MCNP modeled neutron and photon transport. MCNP was run in a source-driven mode, using a fission neutron spatial source created previously for the cycle. In the second case, the intent was to properly model the transport of the delayed photons. In this case, only photons were transported. The same spatial source was modeled as only delayed photons created by the driver fuel were modeled. The energy source was based on a fission product gamma source term. This source term was calculated for the depletion of $PuO_2$ and $UO_2$ in 1971 [43].

The neck-shim rods were modeled as right circular cylinders. To fully insert the rod, its material was switched to hafnium and, to fully remove the rod, its material was switched to aluminum.

A whole core model was taken from the models used for ECAR-4644 [33]. The AFC experiment model was taken from the ECAR-3139 [34].

It was determined that no driver fuel depletion was needed, and only one cycle was modeled. It was determined that only the cases with 0, 3, 5, and 6 neck-shim rods inserted in the lobe needed to be modeled. The neck shims were consecutively inserted, starting from near the center flux trap region, and then moving towards the lobe flux trap region. It was determined that the adjacent experiment needed to be modeled as either an AFC cadmium basket or an SFROP. These scenarios were split into files with only the information for that scenario and then the files were split again into the relevant sections: cells, surfaces, and data. For example, all cards related to the AFC experiment were placed in files, such as `AFC_cells.imcnp`, `AFC_data.imcnp`, etc. A python script then automatically created every permutation of these scenarios, along with the different transport modes, and concatenated these files into separate MCNP input decks.

All model inputs and outputs can be found on the HPC at:
`/projects/experiment_analysis/nsuf/EPRI-ZG/EPRI-ZG-C-as-run-ECAR-5342`.
This folder is a git repository. The repository was on the commit with SHA-1 hash of:
`fdcc5a58202ccafaed8fc1f03cce155968250f2b`.

### 5.1.3 CALCULATING FLUX AND NORMALIZING TALLIES

MCNP flux tallies are normalized per source particle. Therefore, a correction function to calculate flux is based on core power. This function is:

$$\Phi_x(P) = \frac{\bar{\nu}}{Q_f} P \tag{2}$$

where

- $\Phi_x$ is the scalar flux for cell $x$,
- $P$ is the whole core power,
- $\bar{\nu}$ is the average neutrons released per fission,
- $Q_f$ is the energy released per fission (energy lost to neutrinos should not be counted).

For the nuclear heating tallies, the data are reported in units of $\frac{\text{MeV}}{\text{g}}$ and are also normalized to source particles. Due to this, the prompt heating tallies can be normalized in the same way that the flux is normalized using Equation 2. However, for the delayed photon heating, the tally is normalized to the number of delayed photons, not fission neutrons. This must be changed so that it also correlates to core power. Equation 2 can be corrected by the average delayed photons produced per fission:

$$\Phi_{\gamma_d,x}(P) = \frac{\gamma_{d,f}}{Q_f}(P) \tag{3}$$

where $\Phi_{\gamma_d,x}$ is the delayed photon flux in cell $x$ and $\gamma_{d,f}$ is the fission delayed photon yield.

For the radiation damage calculation, the NJOY's quasi-NRT model was used [44]. (The NRT model is a radiation damage model created by Norgett Robinson and Torrens [45]). This is calculated by:

$$\frac{\partial D_x}{\partial t} = \int_0^\infty \eta \frac{\sigma_{d,x}(E)\Phi_x(E)}{2E_d} dE \tag{4}$$

where

- $D$ is the radiation damage "measured" in dpa,
- $\eta$ is the "efficiency" correction factor of 0.8,
- $\sigma_{d,x}$ is the damage-energy-cross section in MeV-barns,
- $E_d$ is the average displacement threshold energy,
- $E$ is the neutron energy.

The damage-energy-cross section was precalculated with NJOY and stored in the material table (MT) 444. A reaction rate tally for MT=444 was used, automatically integrating $\sigma_d(E)\Phi(E)dE$. So, to get the total radiation damage, assuming constant irradiation conditions, all that must be calculated is:

$$D_x = \int_0^T \frac{R_{d,x}(t)\eta}{2E_d} dt \tag{5}$$

where $T$ is the total irradiation time, and $R_d$ is the reaction rate integral found from the tally.

### 5.1.4 RADIATION DAMAGE AND NICKEL

As previously noted in Equation 5. There is a possible time dependence of the reaction rate for radiation damage. There have been no methodical studies examining when this reaction rate is and isn't time dependent. Greenwood has found one case in which this reaction rate is variant with time: when nickel is involved [46][47]. Under irradiation the synthetic isotope Ni-59 is produced. This isotope undergoes extremely exothermic $(n, \alpha)$ and $(n, p)$ reactions. Since Ni-59 is synthetic, it's concentration varies over the irradiation and, therefore, so does the radiation damage rate.

Currently, there is no established method to analytically solve Equation 5. Rather the currently established method is to:

1. Assume a constant radiation damage rate for the entire irradiation.

2. Perform an activation of only the nickel and calculate the helium and hydrogen gasses produced.

3. Correct the radiation damage by adding 1 dpa for every 567 appm He [46] and 1 dpa for every 90 appm H [47] produced in the nickel. For thermal reactors, Greenwood has published an updated helium correction factor that includes $(n, \alpha)$, $(n, p)$, and $(n, \gamma)$ reactions. This correction factor is 1 dpa for every 548 appm He.

So first, for every core configuration, the radiation damage was assumed to constant, simplifying Equation 5 to be:

$$D_x = \frac{\eta}{2E_d} \sum_{i=0}^{I} R_{d,x,i} T_i \tag{6}$$

where the $i$ index is for every unique core configuration and constant-power region. Nickel was activated by itself, and the correlation between weight percent Ni in a sample, and additional radiation damage will be calculated per Greenwood's correlations (1 dpa for every 548 appm He).

### 5.1.5 RADIATION DAMAGE AND PROPRIETARY ALLOYS

Many of the samples in the EPRI-ZG experiment are vendor proprietary alloys, and the exact alloy compositions are not provided. This is problematic as many of the alloying materials (e.g., Ni, Cr, Nb, V), produce different amounts of radiation damage than the base zirconium. This is shown in Figure 2, which compares the damage-energy-cross sections for many of the alloying materials.

Due to this uncertainty, data will be provided for the maximum and minimum feasible amount of radiation damage based on the sample compositions. In addition, radiation damage data will be provided for each alloy constituent and will be normalized to the atom percent of the element. To calculate the total radiation damage, all that is needed is a simple sum:

$$D_x = \sum_{j=0}^{J} \frac{D_{x,j}}{n_j} n_j \tag{7}$$

where

- $\frac{D_{x,j}}{n_j}$ is the radiation damage for alloy constituent $j$ per concentration of constituent,
- $n_j$ is the concentration of alloy constituent $j$.

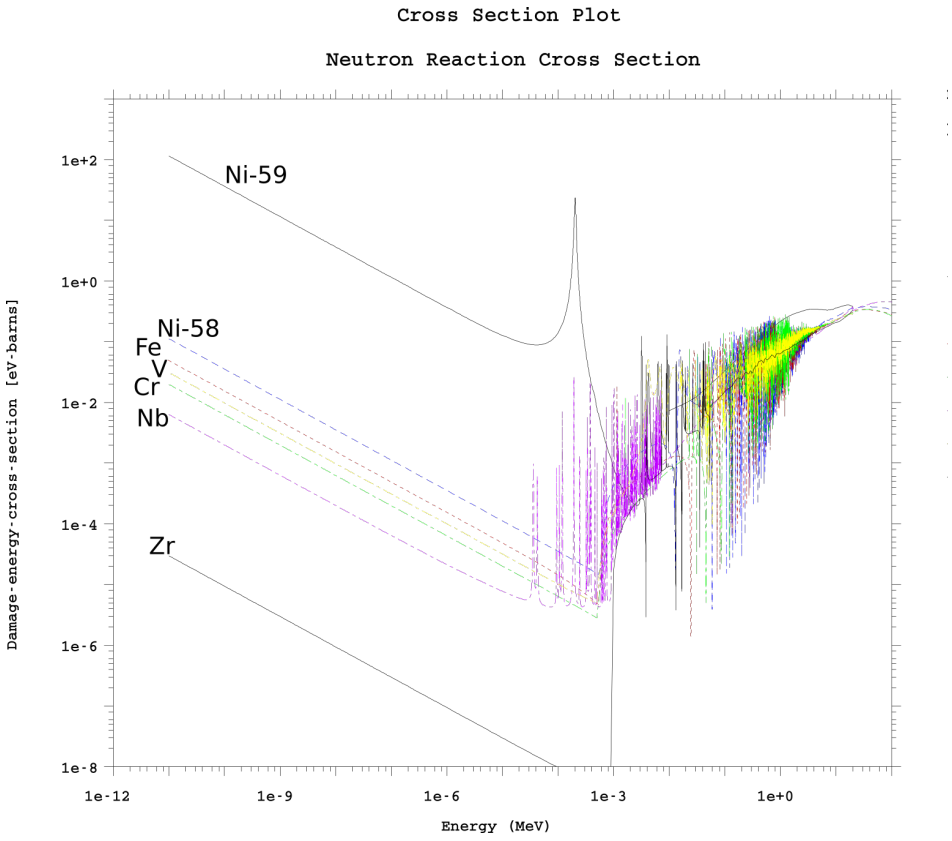


Figure 2: The damage-energy-cross sections for various alloy constituents of zircalloy.

For example: imagine that the values in Table 14 are given. The total radiation can be calculated as:

$$D_x = \frac{D_{x,Zr}}{n_{Zr}} n_{Zr} + \frac{D_{x,Nb}}{n_N b} n_N b + \frac{D_{x,Ni}}{n_{Ni}} n_{Ni} \tag{8}$$

$$D_x = 1 \cdot 0.993 + 10 \cdot 0.002 + 20 \cdot 0.001 \tag{9}$$

$$D_x = 1.033 \tag{10}$$

Table 14: ***Example*** data to be given for radiation damage for showing calculation process.

| **Element** | **normalized Damage** $\left[\frac{\text{dpa}}{\text{at.ratio}}\right]$ | **Concentration** [at.%] |
|---|---|---|
| Zr | 1 | 99.3 |
| Nb | 10 | 0.2 |
| Ni | 20 | 0.1 |

In addition bounding estimates of the maximum, and minimum possible damage accumulations were calculated. For this compositions that would provide the maximum and minimum damage were found. First the data of the damage per atom fraction for nickel was corrected based on Section 5.1.4. The data of the damage per atom for all elements were then ranked in order of the damage production $\left[\frac{\text{dpa}}{\text{at.ratio}}\right]$. Then in order the most damaging element was selected for the maximum damage producing alloy (vice versa for the minimum damage alloy), and that element's composition was set to the maximum allowed for the alloys AG, BG, AW, BW, and AA. This process was continued for the other elements until zirconium was reached, Which then made up the balance of the material. In both cases the zirconium content was above the 97 wt. % threshold stipulated.

### 5.1.6 CALCULATING NU-BAR

For the normalization of the flux tallies, the total average number of fission neutrons released ($\bar{\nu}$) is needed. However, this value is technically energy dependent, so a flux weighted average is needed. For simplicity, it was assumed that only U-235 fissioned in the driver fuel. Also, a simple $\frac{1}{E}$ flux distribution was assumed. This is not truly accurate for ATR as it ignores the fission energy peak and the Maxwell-Boltzmann thermal distribution. However, at thermal energies, $\nu$ is very flat. Data were taken directly from ENDF/B-VII.1 [36]. To avoid being biased towards the extreme ends of the nuclear data, only data in the range: [0.0253 eV, 10 MeV] were used. These were flux-averaged according to:

$$\bar{\nu} = \frac{\int_{E_1}^{E_2} \nu(E) \frac{1}{E} dE}{\int_{E_1}^{E_2} \frac{1}{E} dE} \tag{11}$$

The result of this calculation, along with other important values are presented in Table 15.

Table 15: Constants and input data used for flux normalization.

| **Quantity** | **Value** |
|---|---|
| $Q$ [36] | 193.41 MeV |
| $\bar{\nu}$ [sec 5.1.6] | 2.4367 |
| $\eta$ [45] | 0.8 |
| eV to J [48] | $1.602\,176\,634 \times 10^{-19} \frac{\text{J}}{\text{eV}}$ |
| $\gamma_{d,f}$ [43] | 8.9603 |

Table 16: Normalization factors used for various tallies.

| **Tally Type** | **Normalization Factors** | **Resulting Units** |
|---|---|---|
| Prompt heating | $1.2598 \times 10^{4}$ | $\frac{\text{W}}{\text{gMW}}$ |
| Delayed photon heating | $4.6328 \times 10^{4}$ | $\frac{\text{W}}{\text{gMW}}$ |
| Radiation damage tally | $7.863\,44 \times 10^{-2}$ | $\frac{\text{dpa}}{\text{sMW}}$ |

## 5.2 RESULTS

The majority of the results of this ECAR are stored in Office Open XML workbooks (.xlsx files). These files will be stored with this ECAR in EDMS in a zip file that is included as the "native file". Otherwise, they are available in the HPC file-system at:

`/projects/experiment_analysis/nsuf/EPRI-ZG/EPRI-ZG-C-as-run-ECAR-5342/results`

### 5.2.1 NUCLEAR HEATING

The heating tally data are stored in three distinct files: `samples.xlsx`, `spacers.xlsx`, and `structure.xlsx`. Each file contains many spreadsheets corresponding to the core configuration simulation (e.g., the sheet: `166B1-0Necks-AFC`, corresponds to the case where no neck shim rods were inserted, and the AFC cadmium basket was the experiment next to this capsule). The column "layer" corresponds to the row modeled, with Layer 1 being the bottom-most row (i.e., nearest the coolant outlet). In the column headers, "N" corresponds to neutron heating and "P" corresponds to photon heating. The relevant "_uncert" columns are the uncertainties on these values reported by MCNP. These uncertainties are relative, and are not in per-cent.

For the structural materials, the names cells were given were somewhat ambiguous. In this case, using the MCNP cell numbers is useful. MCNP geometry plots with the cell numbers superimposed are given in Figure 3 for the cells at the top of the capsule, and in Figure 5 for the cells at the bottom of the capsule.

Summary data were also provided. These data are available in: `HeatingSummarysamples.xlsx`, `HeatingSummaryspacers.xlsx`, and `HeatingSummarystructure.xlsx`. These are similarly broken into samples, sample spacers, and not experimental structural components respectively. Each spreadsheet in the workbooks represent a single cycle. For each cycle the cycle-averaged powers were found for the whole core, and the relevant lobe powers (based on NDMAS data). The core power was then corrected factor to account for the real core power split versus the one modeled in MCNP. Then for each cycle the different neck shim rod configurations were multiplied by the average core powers. The data are then reported in specific power $\left[\frac{\mathrm{W}}{\mathrm{g}}\right]$. Next for each cell the powers for each neck shim rod configuration were arithmetically averaged, this was *not* a weighted average. The maximum heating rate was found as well. For the samples this was applied to all samples on that layer as well. That is the reported average for a layer is the average of the averages calculated for each sample. The maximum is the maximum heating rate across all samples and configurations for that sample layer.

### 5.2.2 RADIATION DAMAGE

Detailed information on the radiation damage rates is located in the `DamageRate.xlsx` workbook. The spreadsheets follow the same naming format as the nuclear heating workbooks. The "_uncert" columns are also relative uncertainties. The data are reported in units of $\frac{\mathrm{dpa}}{\mathrm{at.\%sMW}}$ The data were only measured for three spatial areas representing the top middle and bottom or "lower" rows in the capsule. These correspond to rows 10 5 and 1, respectively. These data are based on assuming a constant damage rate and do not include the nickel correction factor.

These data along with the irradiation history were used to calculate the total radiation damage using Equation 7. These data are presented in Table 17.

The nickel correction was found by activating Ni by itself and measuring the accumulated He gas. These data are given in Table 18. The Ni correction factors based on hydrogen gas production are impractically large ($\sim 6\frac{\mathrm{dpa}}{\mathrm{at.\%}}$). Clearly there is another source of hydrogen gas other than the Ni-59 $(n,p)$ reaction, so the hydrogen data were not used. Instead, the updated He-based nickel correction factor of 1 dpa per 548 appm He was used [46].

Table 17: The uncorrected radiation damage by constituent element. These data are given in $\frac{\text{dpa}}{\text{at.ratio}}$. The positions top, middle, and lower correspond to Rows 10, 5, and 1, respectively.

| Element | Top | Middle | Lower |
|---|---|---|---|
| Sn | 13.5 | 14.5 | 13.5 |
| Nb | 17.7 | 18.9 | 17.6 |
| Fe | 17.4 | 18.6 | 17.3 |
| Cr | 19.4 | 20.8 | 19.3 |
| Ni | 19.6 | 21.0 | 19.5 |
| V | 23.3 | 25.0 | 23.2 |
| O | 20.6 | 22.2 | 20.6 |
| H | 1.7 | 1.8 | 1.7 |
| Zr | 18.7 | 20.1 | 18.6 |

Table 18: Data needed for implementing the nickel correction factor for radiation damage [46][47].

| Capsule Position | H Production $\left[\frac{\text{appm}}{\text{at.\%Ni}}\right]$ | He Production $\left[\frac{\text{appm}}{\text{at.\%Ni}}\right]$ | Damage Correction $\left[\frac{\text{dpa}}{\text{at.\%Ni}}\right]$ |
|---|---|---|---|
| Top | $1.56 \times 10^2$ | $3.92 \times 10^1$ | 0.0716 |
| Middle | $1.55 \times 10^2$ | $3.94 \times 10^1$ | 0.0719 |
| Lower | $1.54 \times 10^2$ | $3.85 \times 10^1$ | 0.0702 |

Due to the exact alloy compositions being unknown to the Laboratory calculating exact values for the damage accumulation in each sample is not possible. Instead estimates for the maximum, and minimum possible damage accumulations were calculated. For this compositions that would provide the maximum and minimum damage were found. First the data from Table 17 were updated with the nickel correction factors in Table 18 according to Section 5.1.4. These data were then ranked in order of the damage production $\left[\frac{\text{dpa}}{\text{at.ratio}}\right]$. Then in order, the most damaging element was selected for the maximum damage producing alloy (vice versa for the minimum damage alloy), and that element's composition was set to the maximum allowed for the alloys AG, BG, AW, BW, and AA. This process was continued for the other elements until zirconium was reached, Which then made up the balance of the material. In both cases the zirconium content was above the 97 wt. % threshold. These compositions and the calculated extreme damage values are presented in Table 19.

Table 19: The maximum and minimum possible radiation damage accumalation for samples composed of alloys AG, BG, AW, BW, and AA. Compositions were postulated based on provided data that would maximimze and minimize the accumulation of damage. The compositions for these postulated alloys are given in wt. %.

| | Composition | Top | Middle | Lower |
|---|---|---|---|---|
| **Maximum Damage** | Zr-0.1V-0.2O-0.1Ni-0.1Cr | 18.7 | 20.1 | 18.6 |
| **Minimum Damage** | Zr-0.0125H-1.2Sn-1.2Fe-1.2Nb | 18.4 | 19.8 | 18.3 |

### 5.2.3 ACTIVATION

The activation was performed using the COUPLE and ORIGEN modules of SCALE-6.2.3, with the assistance of the MOAA script. These data were then combined into two workbooks specifically targeting the needs of shipping and MFC operations (`ShippingData.xlsx` and `MFCdata.xlsx`).

First, the shipping report was meant to support shipping by creating a total source term for the entirety of the capsule, which would be shipped in the cask after resizing. This workbook (`shippingData.xlsx`) is comprised of three spreadsheets, each of which presents a different set of data. The "Grams" sheet presents the capsule's isotopic compositions (stable and radioactive) in units of grams. This sheet is intended to be used by MFC operations, and not shipping. It is included in this workbook though to avoid confusion of whether or not the data are for the entire capsule. The "Curies" sheet presents the capsule's radioactivity in units of curies. The "WATTS" sheet presents the decay heat source term for the capsule in watts, including all heat sources. The "GAMWATTS" sheets presents the decay heat source term, which is transported by gamma photons. For all data types, the data presented is the sum total for the whole capsule. The first column presents the source isotope (or isomer) in question. The remaining columns are days since the EOI. See Table 3 for which dates these cooldown periods correspond to.

Finally, the MFC report is meant to support MFC HFEF operations after capsule disassembly. Therefore, only materials which will be kept for later examination are included. These are the actual zircalloy samples, the melt wire capsules, and the SiC temperature monitors. In this workbook, all of the data are of the same type: the radioactivity content of these samples by mass in grams. In this case, the data are for one single specimen of each type; each spreadsheet refers to a different type. The "sample" sheet contains the data for the zircalloy samples. The "meltWire" sheet contains the data for the melt-wire capsules. The "tempMonitor" sheet contains the data for the SiC temperature monitors. All of the data represent the maximum feasible radionuclide inventory. All of the data for samples of that kind were combined, and then the maximum value for each isotope (or isomer) was taken. The actual spreadsheet structure is similar to the shipping workbook ones. The first column represents the isotope (or isomer). The remaining columns are the days from the EOI.

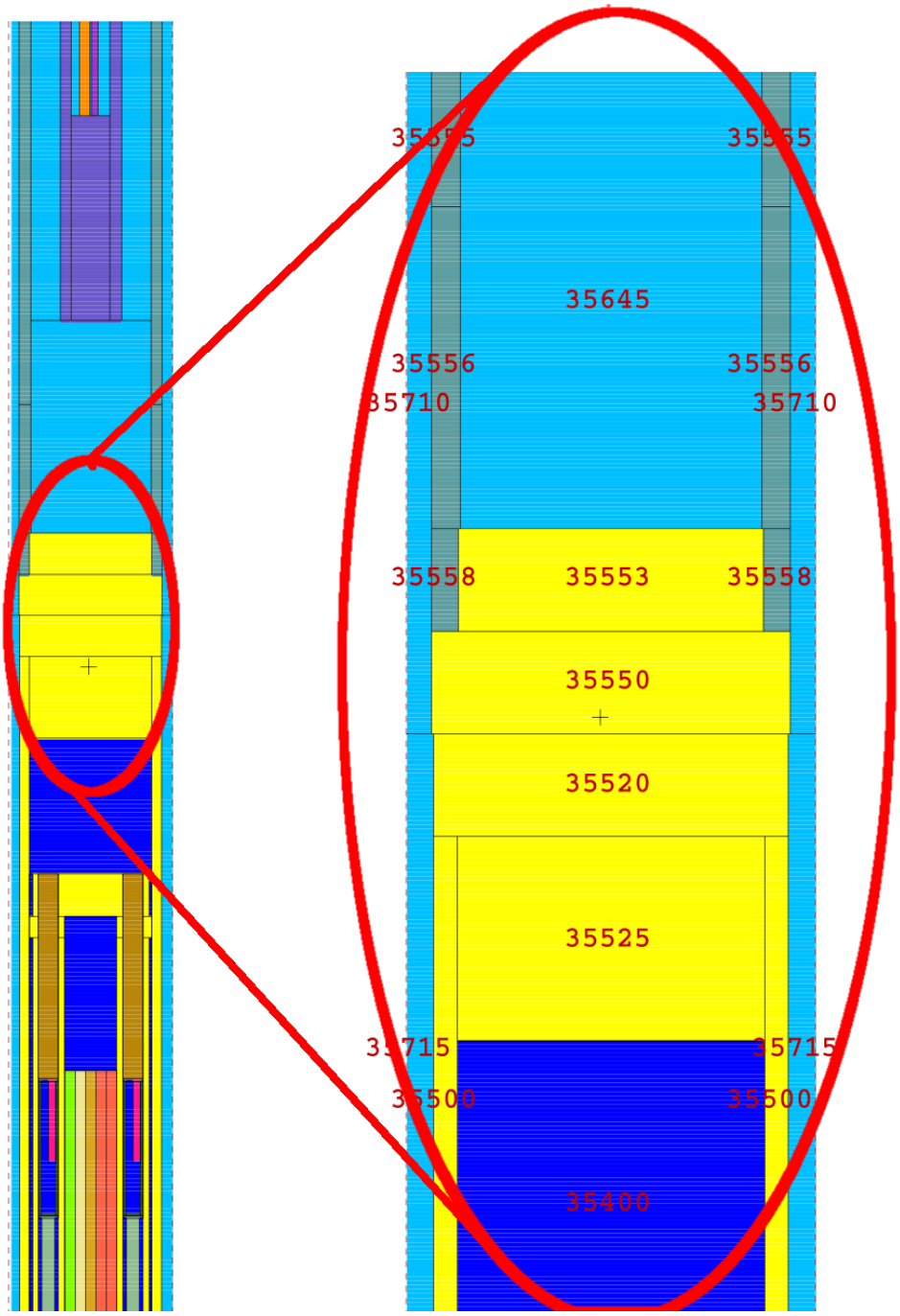


Figure 3: A geometry plot with cell numbers from MCNP of the top of the capsule. The yellow cells are the steel of the capsule and sample holder, the light blue cells are the reactor coolant, and the sage-green cells are the steel tubes for the basket.

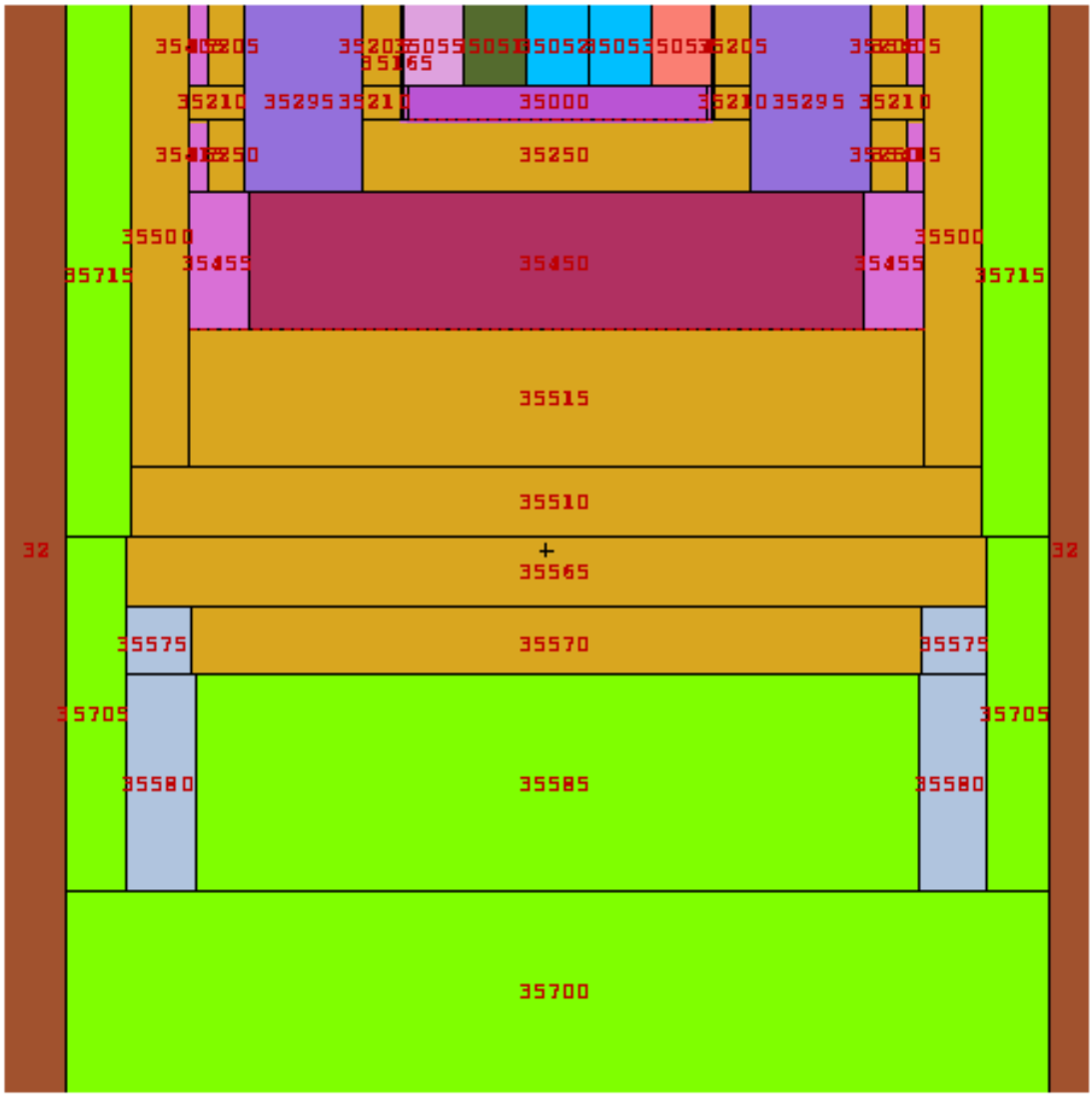


Figure 4: A geometry plot with cell numbers from MCNP of the bottom of the capsule cut along the X-Z plane. The yellow-orange cells are the steel of the capsule and sample holder, the neon green cells are the reactor coolant, and the pale blue cells are the steel tubes for the basket. The light blue cell, 35053 is a sample. Note that for legibility the plot has been stretched disproportionately in the X direction.

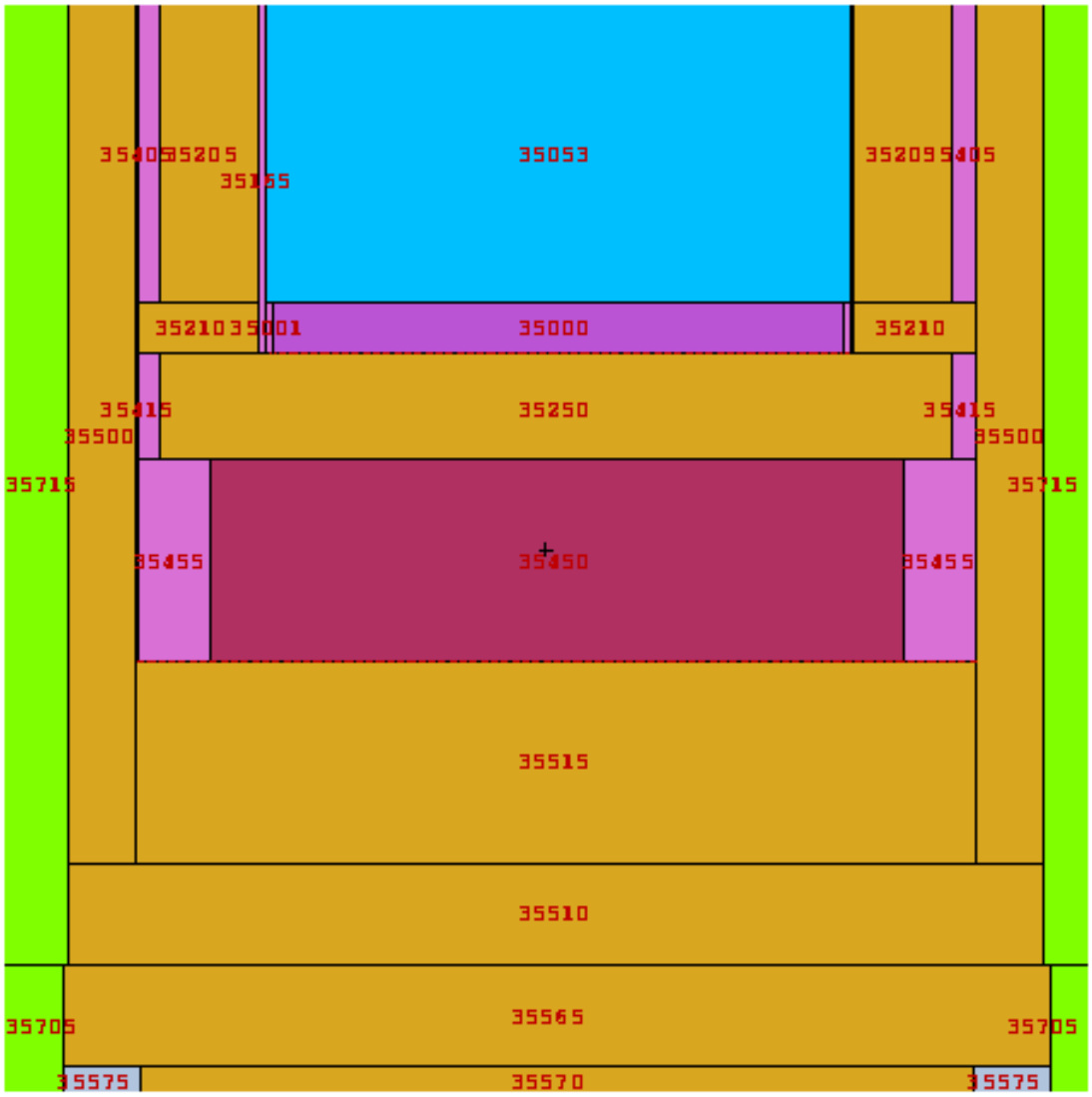


Figure 5: A geometry plot with cell numbers from MCNP of the bottom of the capsule cut along the Y-Z plane. The yellow-orange cells are the steel of the capsule and sample holder, the neon green cells are the reactor coolant, and the pale blue cells are the steel tubes for the basket. Note that for legibility the plot has been stretched disproportionately in the X direction.

# 6 REFERENCES

## References

[1] "Irradiation test plan project number: 30178 EPRI zirconium growth experiment," Idaho National Laboratory, Idaho Falls, ID, INL Test Plan PLN-3303, Feb. 3, 2011.

[2] S. Yagnik, "The NFIR-v dimensional stability project: Material variants for irradiation in BOR-60," Electric Power Research Institute, Palo Alto, CA, EPRI Report 1013433, Dec. 2006, pp. 2-3 –2-4.

[3] N. Oldham, "ATR core cross section diagrams," Idaho National Lab. (INL), Idaho Falls, ID, INL Drawing 60600, p. 2.

[4] D. Dempsey and C. Murdock, *AFC outboard-a experiments cadmium baskets*, E-mail, Oct. 14, 2020.

[5] S. Jensen, "ATR OUTBOARD AND INBOARD "a" POSITION SPECIMEN FILLER PLUGS DETAILS SHEET 1 ALTERNATE ID: ATR-1075-MTR-670-m-237," Idaho National Laboratory, Idaho Falls, ID, Drawing 120421, Apr. 30, 2013.

[6] J. Poling, "Results of reactor physics safety analysis for advanced test reactor cycle 152b-1," Idaho National Lab. (INL), Idaho Falls, ID, ECAR-2080, Nov. 5, 2012. [Online]. Available: https://inl-edms.inl.gov/pls/inl_docs/doc_3?f_doc=ECAR-2080.

[7] P. A. Roth, "RESULTS OF REACTOR PHYSICS SAFETY ANALYSIS FOR ADVANCED TEST REACTOR (ATR) CYCLE 149b," Idaho National Lab. (INL), Idaho, ECAR 1524, May 26, 2011. [Online]. Available: https://inl-edms.inl.gov/pls/inl_docs/doc_3?f_doc=ECAR-1524.

[8] M. A. ( Plummer and N. ( Johnson, "NDMAS system and process description," Idaho National Lab. (INL), Idaho Falls, ID (United States), INL/MIS-20-58046-Rev000, Apr. 27, 2020. [Online]. Available: https://www.osti.gov/biblio/1634835-ndmas-system-process-description (visited on 12/18/2020).

[9] *EPRI-ZG-c as-run ECAR follow-on requirements*, in collab. with A. Tam, S. Wilson, C. Xing, S. Case, J. Peterson-Droogh, M. Arrowood, and J. Mitchell, E-mail, Dec. 10, 2020.

[10] A. W. LaPorta, "Results of reactor physics safety analysis for advanced test reactor (ATR) cycle 150b," Idaho National Lab. (INL), Idaho Falls, ID, ECAR-1660, Aug. 31, 2011. [Online]. Available: https://inl-edms.inl.gov/pls/inl_docs/doc_3?f_doc=ECAR-1660.

[11] B. Curnutt, "Results of reactor physics safety analysis for advanced test reactor cycle 151a," Idaho National Lab. (INL), Idaho Falls, ID, ECAR-1742, Dec. 8, 2011. [Online]. Available: https://inl-edms.inl.gov/pls/inl_docs/doc_3?f_doc=ECAR-1742.

[12] P. Roth, "Results of reactor physics safety analysis for advanced test reactor (ATR) cycle 151b," Idaho National Lab. (INL), Idaho Falls, ID, ECAR-1804, Feb. 21, 2012. [Online]. Available: https://inl-edms.inl.gov/pls/inl_docs/doc_3?f_doc=ECAR-1804.

[13] M. Morrison, "Results of reactor physics safety analysis for advanced test reactor cycle 155b-1," Idaho National Lab. (INL), Idaho Falls, ID, ECAR-2436, Jan. 13, 2014. [Online]. Available: https://inl-edms.inl.gov/pls/inl_docs/doc_3?f_doc=ECAR-2436.

[14] "Reactor loading record for ATR cycle 158b-1," Idaho National Lab. (INL), Idaho Falls, ID, 158B-1, Feb. 1, 2016. [Online]. Available: https://inl-edms.inl.gov/pls/inl_docs/doc_3?f_doc=158B-1.

[15] "Reactor loading record for ATR cycle 160b-1," Idaho National Lab. (INL), Idaho Falls, ID, 160B-1, Nov. 14, 2016. [Online]. Available: https://inl-edms.inl.gov/pls/inl_docs/doc_3?f_doc=160B-1.

[16] "Reactor loading record for ATR cycle 162b-1," Idaho National Lab. (INL), Idaho Falls, ID, 162B-1, Dec. 7, 2017. [Online]. Available: https://inl-edms.inl.gov/pls/inl_docs/doc_3?f_doc=162B-1.

[17] "Reactor loading record for ATR cycle 164a-1," Idaho National Lab. (INL), Idaho Falls, ID, 164A-1, May 17, 2018. [Online]. Available: https://inl-edms.inl.gov/pls/inl_docs/doc_3?f_doc=164A-1.

[18] "Reactor loading record for ATR cycle 164b-1," Idaho National Lab. (INL), Idaho Falls, ID, 164B-1, Jan. 16, 2019. [Online]. Available: https://inl-edms.inl.gov/pls/inl_docs/doc_3?f_doc=164B-1.

[19] "Reactor loading record for ATR cycle 168a-1," Idaho National Lab. (INL), Idaho Falls, ID, 168A-1, Mar. 26, 2020. [Online]. Available: https://inl-edms.inl.gov/pls/inl_docs/doc_3?f_doc=168A-1.

[20] "Reactor loading record for ATR cycle 168b-1," Idaho National Lab. (INL), Idaho Falls, ID, 168B-1, Jul. 20, 2020. [Online]. Available: https://inl-edms.inl.gov/pls/inl_docs/doc_3?f_doc=168B-1.

[21] "Standard specification for aluminum and aluminum-alloy drawn seamless tubes," ASTM International, West Conschohocken, PA, Standard B210/B201M - 19a, Nov. 1, 2019.

[22] "Standard specification for stainless steel bars and shapes," ASTM International, West Conschohocken, PA, A276/A276M - 17, Mar. 15, 2017.

[23] "Standard specification for seamless ferritic and austenitic alloy-steel boiler, superheater, and heat-exchanger tubes1," ASTM International, West Conschohocken, PA, A213/A214M - 19a, Dec. 1, 2019.

[24] "Standard specification for stainless steel bars and shapes for use in boilers and other pressure vessels," ASTM International, West Conschohocken, PA, A479/A479M - 20, Jul. 1, 2020.

[25] M. Wang, G. Audi, F. G. Kondev, W. Huang, S. Naimi, and X. Xu, "The AME2016 atomic mass evaluation (II). tables, graphs and references," *Chinese Physics C*, vol. 41, no. 3, p. 030 003, Mar. 2017, ISSN: 1674-1137. DOI: 10.1088/1674-1137/41/3/030003. [Online]. Available: https://iopscience.iop.org/article/10.1088/1674-1137/41/3/030003 (visited on 01/14/2021).

[26] J. Meija, T. B. Coplen, M. Berglund, W. A. Brand, P. De Bièvre, M. Gröning, N. E. Holden, J. Irrgeher, R. D. Loss, T. Walczyk, and T. Prohaska, "Isotopic compositions of the elements 2013 (IUPAC technical report)," *Pure and Applied Chemistry*, vol. 88, no. 3, pp. 293–306, Mar. 1, 2016, ISSN: 1365-3075, 0033-4545. DOI: 10.1515/pac-2015-0503. [Online]. Available: https://www.degruyter.com/view/journals/pac/88/3/article-p293.xml (visited on 01/14/2021).

[27] *The International System of Units (SI)*, 9th ed. Paris, France: Bureau International des Poids et Mesures, 2019, 102 pp., ISBN: 978-92-822-2272-0. [Online]. Available: https://www.bipm.org/utils/common/pdf/si-brochure/SI-Brochure-9-EN.pdf (visited on 07/30/2019).

[28] C. L. Whitmarsh, "REVIEW OF ZIRCALOY-2 AND ZIRCALOY-4 PROPERTIES RELEVANT TO n.s. SAVANNAH REACTOR DESIGN," ORNL-3281, 4827123, Jul. 23, 1962, ORNL–3281, 4 827 123. DOI: 10.2172/4827123. [Online]. Available: http://www.osti.gov/servlets/purl/4827123/ (visited on 09/23/2020).

[29] "Wrought stainless steels," in *Properties and Selection: Irons, Steels, and High-Performance Alloys*, ASM International, 1990, pp. 841–907, ISBN: 978-1-62708-161-0. DOI: 10.31399/asm.hb.v01.a0001046. [Online]. Available: https://dl.asminternational.org/books/book/16/chapter/251054/wrought-stainless-steels (visited on 09/23/2020).

[30] "Aluminum mill and engineered wrought products," in *Properties and Selection: Nonferrous Alloys and Special-Purpose Materials*, ASM International, 1990, pp. 29–61, ISBN: 978-1-62708-162-7. DOI: 10.31399/asm.hb.v02.a0001059. [Online]. Available: https://dl.asminternational.org/books/book/14/chapter/199830/aluminum-mill-and-engineered-wrought-products (visited on 09/23/2020).

[31] "Properties of pure metals," in *Properties and Selection: Nonferrous Alloys and Special-Purpose Materials*, ASM International, 1990, pp. 1099–1201, ISBN: 978-1-62708-162-7. DOI: 10.31399/asm.hb.v02.a0001117. [Online]. Available: https://dl.asminternational.org/books/book/14/chapter/214667/properties-of-pure-metals (visited on 09/30/2020).

[32] "Engineering tables: Ceramics and glasses," in *Engineered Materials Handbook Desk Edition*, M. M. Gauthier, Ed., ASM International, 1995, pp. 103–105, ISBN: 978-1-62708-200-6. DOI: 10.31399/asm.hb.emde.a0003004. [Online]. Available: https://dl.asminternational.org/books/book/48/chapter/556204/engineering-tables-ceramics-and-glasses (visited on 09/23/2020).

[33] E. T. Swain, "ATR cycle 166a projected physics analysis for the AFC experiments irradiated in the ATR outboard a irradition positions," Idaho National Lab. (INL), Idaho Falls, ID, ECAR - 4644, Jul. 18, 2019. [Online]. Available: https://inl-edms.inl.gov/pls/inl_docs/doc_3?f_doc=ECAR-4644.

[34] D. O. Choe., "PHYSICS ANALYSIS TO DESIGN u-235 ENRICHMENT VALUES OF METALLIC URANIUM FUELS FOR THE AFC-3f EXPERIMENT IRRADIATED IN THE ATR a-11 OUTBOARD a POSITION," Idaho National Lab. (INL), Idaho Falls, ID, ECAR-3139, Feb. 25, 2016. [Online]. Available: https://inl-edms.inl.gov/pls/inl_docs/doc_3?f_doc=ECAR-3139.

[35] H. Lemmel, P. McLaughlin, and V. Pronyaev, "ENDF/b-VI release 8 (last release of ENDF/b-VI) the u.s. evaluated nuclear data library for neutron reaction data," International Atomic Energy Agency: Nuclear Data Services, IAEA-NDS-100, Nov. 2001. [Online]. Available: https://www.nndc.bnl.gov/endf/b6.8/doc/NDS-100.pdf.

[36] M. Chadwick, M. Herman, P. Obložinský, M. Dunn, Y. Danon, A. Kahler, D. Smith, B. Pritychenko, G. Arbanas, R. Arcilla, R. Brewer, D. Brown, R. Capote, A. Carlson, Y. Cho, H. Derrien, K. Guber, G. Hale, S. Hoblit, S. Holloway, T. Johnson, T. Kawano, B. Kiedrowski, H. Kim, S. Kunieda, N. Larson, L. Leal, J. Lestone, R. Little, E. McCutchan, R. MacFarlane, M. MacInnes, C. Mattoon, R. McKnight, S. Mughabghab, G. Nobre, G. Palmiotti, A. Palumbo, M. Pigni, V. Pronyaev, R. Sayer, A. Sonzogni, N. Summers, P. Talou, I. Thompson, A. Trkov, R. Vogt, S. van der Marck, A. Wallner, M. White, D. Wiarda, and P. Young, "ENDF/b-VII.1 nuclear data for science and technology: Cross sections, covariances, fission product yields and decay data," *Nuclear Data Sheets*, vol. 112, no. 12, pp. 2887–2996, Dec. 2011, ISSN: 00903752. DOI: 10.1016/j.nds.2011.11.002. [Online]. Available: https://linkinghub.elsevier.com/retrieve/pii/S009037521100113X (visited on 10/21/2019).

[37] J. W. Nielsen, "VERIFICATION AND VALIDATION TESTING OF MCNP AND ORIGEN2 COMPUTER CODES FOR IDAHO NATIONAL LABORTORY (INL) HIGH PERFORMANCE COMPUTING (HPC) SYSTEMS," Idaho National Lab. (INL), Idaho Falls, ID (United States), Technical Evaluation TEV-2944, Jul. 16, 2019. [Online]. Available: https://inl-edms.inl.gov/pls/inl_docs/doc_3?f_doc=TEV-2944.

[38] J. Peterson-Droogh, "VERIFICATION AND VALIDATION TESTING OF SCALE6/ORIGENS APPLICATION," Idaho National Lab. (INL), Idaho Falls, ID, Technical Evaluation TEV-3686, Sep. 23, 2019. [Online]. Available: https://inl-edms.inl.gov/pls/inl_docs/doc_3?f_doc=TEV-3686.

[39] J. T. Goorley, M. R. James, T. E. Booth, J. S. Bull, L. J. Cox, J. W. J. Durkee, J. S. Elson, M. L. Fensin, R. A. I. Forster, J. S. Hendricks, H. G. I. Hughes, R. C. Johns, B. C. Kiedrowski, R. L. Martz, S. G. Mashnik, G. W. McKinney, D. B. Pelowitz, R. E. Prael, J. E. Sweezy, L. S. Waters, T. Wilcox, and A. J. Zukaitis, "Initial MCNP6 release overview - MCNP6 version 1.0," LA-UR-13-22934, 1086758, Jun. 26, 2013, LA–UR–13–22 934, 1 086 758. DOI: 10.2172/1086758. [Online]. Available: http://www.osti.gov/servlets/purl/1086758/ (visited on 01/17/2021).

[40] B. T. Rearden, M. E. Dunn, D. Wiarda, C. Celik, K. B. Bekar, M. L. Williams, D. E. Peplow, C. M. Perfetti, I. C. Gauld, W. A. Wieselquist, J. P. Lefebvre, R. A. Lefebvre, F. Havluj, S. Skutnik, and K. Dugan, "OVERVIEW OF SCALE 6.2," OSTI Report 1095656, 2013. [Online]. Available: https://www.osti.gov/biblio/1095656.

[41] G. v. Rossum, "Python tutorial," Centrum voor Wiskunde en Informatica, Amsterdam, the Netherlands, CS-R9526, 1995. [Online]. Available: https://ir.cwi.nl/pub/5007/05007D.pdf.

[42] C. J. Soloman, C. Bates, and J. Kulesza, "The MCNPTools package: Installation and use," Las Alamos National Laboratory, Las Alamos, N. M., LA-UR-17-21779, Mar. 30, 2017.

[43] E. T. Boulette and W. L. Bunch, "ANALYSIS OF ZPPR/FTR SHIELD EXPERIMENTS: GAMMA DISTRIBUTION.," WHAN-FR-13, 4012626, Jan. 1, 1971, WHAN–FR–13, 4 012 626. DOI: 10.2172/4012626. [Online]. Available: http://www.osti.gov/servlets/purl/4012626/ (visited on 08/12/2020).

[44] R. E. MacFarlane, D. W. Muir, R. M. Boicourt, A. C. Kahler, J. L. Conlin, and W. Haeck, "The NJOY nuclear data processing system, version 2016," Las Alamos National Laboratory, Las Alamos, N. M., Government Manual LA-UR-17-20093, Jul. 3, 2018. DOI: 10.2172/1338791. [Online]. Available: https://doi.org/10.2172/1338791 (visited on 08/01/2019).

[45] M. Norgett, M. Robinson, and I. Torrens, "A proposed method of calculating displacement dose rates," *Nuclear Engineering and Design*, vol. 33, no. 1, pp. 50–54, Aug. 1975, ISSN: 00295493. DOI: 10.1016/0029-5493(75)90035-7. [Online]. Available: https://linkinghub.elsevier.com/retrieve/pii/0029549375900357 (visited on 08/06/2019).

[46] L. Greenwood, "A new calculation of thermal neutron damage and helium production in nickel," *Journal of Nuclear Materials*, vol. 115, no. 2, pp. 137–142, Apr. 1983, ISSN: 00223115. DOI: 10.1016/0022-3115(83)90302-1. [Online]. Available: https://linkinghub.elsevier.com/retrieve/pii/0022311583903021 (visited on 07/29/2019).

[47] L. Greenwood and F. Garner, "Hydrogen generation arising from the59ni(n, p) reaction and its impact on fission—fusion correlations," *Journal of Nuclear Materials*, vol. 233-237, pp. 1530–1534, Oct. 1996, ISSN: 00223115. DOI: 10.1016/S0022-3115(96)00264-4. [Online]. Available: https://linkinghub.elsevier.com/retrieve/pii/S0022311596002644 (visited on 09/25/2019).

[48] (). CODATA value: Electron volt, The NIST Reference on Constants, Units, and Uncertainty, [Online]. Available: https://physics.nist.gov/cgi-bin/cuu/Value?evj (visited on 01/17/2021).

# A SIMPLIFIED IRRADIATION HISTORY FOR EPRI-ZG-C

Table 20: The irradiation history for EPRI-ZG-C simplified into constant-power sections. Note: SFROP was substituted for the HSA cobalt assembly.

| Cycle | Time [d] | Neck-Shim Rods Inserted | Lobe Power [MW] | Total Power [MW] | Mod-eled Core Split[–] | Lobe Cor-rected To-tal Power [MW] | Adja-cent Loading |
|---|---|---|---|---|---|---|---|
| 149B | 0.44 | 6 | 8.10 | 37.95 | 0.22 | 37.54 | SFROP |
| 149B | 16 | 6 | 22.98 | 105.01 | 0.22 | 106.48 | SFROP |
| 149B | 7 | 5 | 22.97 | 105.42 | 0.22 | 105.83 | SFROP |
| 149B | 12 | 3 | 22.98 | 105.75 | 0.22 | 105.22 | SFROP |
| 149B | 18.38 | 0 | 22.95 | 106.71 | 0.22 | 105.23 | SFROP |
| 149B-out | 77 | -1 | 0.00 | 0.00 | 0.00 | 0.00 | None |
| 150B | 0.68 | 6 | 10.72 | 49.39 | 0.21 | 50.00 | AFC |
| 150B | 1 | 6 | 23.20 | 105.83 | 0.21 | 108.20 | AFC |
| 150B | 12.66 | 5 | 23.00 | 107.68 | 0.22 | 106.82 | AFC |
| 150B | 11 | 3 | 23.06 | 108.07 | 0.22 | 105.56 | AFC |
| 150B | 16.42 | 0 | 23.05 | 108.37 | 0.22 | 106.63 | AFC |
| 150B-out | 18 | -1 | 0.00 | 0.00 | 0.00 | 0.00 | None |
| 151A | 0.96 | 6 | 17.45 | 77.15 | 0.21 | 81.38 | AFC |
| 151A | 10.39 | 6 | 22.97 | 99.33 | 0.21 | 107.13 | AFC |
| 151A | 2.79 | 6 | 0.45 | 2.06 | 0.21 | 2.10 | AFC |
| 151A | 0.82 | 6 | 15.40 | 68.05 | 0.21 | 71.82 | AFC |
| 151A | 3 | 6 | 22.99 | 100.47 | 0.21 | 107.24 | AFC |
| 151A | 3 | 5 | 23.02 | 101.11 | 0.22 | 106.89 | AFC |
| 151A | 13 | 3 | 23.72 | 101.72 | 0.22 | 108.59 | AFC |
| 151A | 25.42 | 0 | 23.96 | 102.66 | 0.22 | 110.80 | AFC |
| 151A-out | 19 | -1 | 0.00 | 0.00 | 0.00 | 0.00 | None |
| 151B | 0.73 | 6 | 16.00 | 72.04 | 0.21 | 74.62 | AFC |
| 151B | 20.3 | 6 | 23.02 | 101.28 | 0.21 | 107.35 | AFC |
| 151B-out | 3.04 | -1 | 0.00 | 0.00 | 0.00 | 0.00 | None |
| 151B | 0.66 | 6 | 16.21 | 72.83 | 0.21 | 75.60 | AFC |
| 151B | 1.56 | 6 | 23.01 | 101.46 | 0.21 | 107.30 | AFC |
| 151B-out | 10.4 | -1 | 0.00 | 0.00 | 0.00 | 0.00 | None |
| 151B | 0.04 | 6 | 1.64 | 7.02 | 0.21 | 7.65 | AFC |
| 151B | 1 | 6 | 20.14 | 90.00 | 0.21 | 93.93 | AFC |
| 151B | 13 | 6 | 23.11 | 101.95 | 0.21 | 107.79 | AFC |
| 151B | 4 | 5 | 23.07 | 102.16 | 0.22 | 107.11 | AFC |

Table 20: (continued).

| Cycle | Time [d] | Neck-Shim Rods Inserted | Lobe Power [MW] | Total Power [MW] | Modeled Core Split[–] | Lobe Corrected Total Power [MW] | Adjacent Loading |
|---|---|---|---|---|---|---|---|
| 151B | 4 | 3 | 23.01 | 101.87 | 0.22 | 105.35 | AFC |
| 151B | 6.38 | 0 | 23.06 | 102.06 | 0.22 | 106.64 | AFC |
| 151B-out | 206 | -1 | 0.00 | 0.00 | 0.00 | 0.00 | None |
| 152B | 0.07 | 6 | 1.10 | 3.58 | 0.22 | 5.10 | SFROP |
| 152B | 1 | 6 | 11.92 | 53.00 | 0.22 | 55.24 | SFROP |
| 152B | 30.9 | 6 | 23.00 | 103.32 | 0.22 | 106.57 | SFROP |
| 152B | 4 | 5 | 23.02 | 103.38 | 0.22 | 106.08 | SFROP |
| 152B | 15.42 | 3 | 22.95 | 103.71 | 0.22 | 105.06 | SFROP |
| 152B-out | 391 | -1 | 0.00 | 0.00 | 0.00 | 0.00 | None |
| 155B | 0.8 | 6 | 13.08 | 59.07 | 0.21 | 61.00 | AFC |
| 155B | 32 | 6 | 22.95 | 104.36 | 0.21 | 107.05 | AFC |
| 155B | 3.26 | 5 | 22.90 | 105.01 | 0.22 | 106.37 | AFC |
| 155B-out | 4.2 | -1 | 0.00 | 0.00 | 0.00 | 0.00 | None |
| 155B | 0.3 | 5 | 4.08 | 18.36 | 0.22 | 18.95 | AFC |
| 155B | 1 | 5 | 22.77 | 104.58 | 0.22 | 105.74 | AFC |
| 155B | 13.13 | 3 | 22.95 | 105.11 | 0.22 | 105.98 | AFC |
| 155B-out | 668 | -1 | 0.00 | 0.00 | 0.00 | 0.00 | None |
| 158B | 0.16 | 6 | 3.62 | 16.39 | 0.21 | 16.88 | AFC |
| 158B | 1 | 6 | 20.86 | 91.56 | 0.21 | 97.29 | AFC |
| 158B | 8 | 6 | 22.90 | 100.19 | 0.21 | 106.81 | AFC |
| 158B | 4 | 5 | 23.03 | 101.14 | 0.22 | 106.93 | AFC |
| 158B | 38.33 | 3 | 23.07 | 101.70 | 0.22 | 105.64 | AFC |
| 158B-out | 263 | -1 | 0.00 | 0.00 | 0.00 | 0.00 | None |
| 160B | 1 | 6 | 17.71 | 85.03 | 0.21 | 82.60 | AFC |
| 160B | 7 | 6 | 23.04 | 108.32 | 0.21 | 107.46 | AFC |
| 160B | 4 | 5 | 23.03 | 107.76 | 0.22 | 106.94 | AFC |
| 160B | 17.7 | 3 | 23.01 | 108.16 | 0.22 | 105.33 | AFC |
| 160B-out | 5.18 | -1 | 0.00 | 0.00 | 0.00 | 0.00 | None |
| 160B | 0.11 | 3 | 2.76 | 12.81 | 0.22 | 12.64 | AFC |
| 160B | 1 | 3 | 19.73 | 93.32 | 0.22 | 90.33 | AFC |
| 160B | 29.6 | 3 | 22.99 | 108.24 | 0.22 | 105.28 | AFC |
| 160B-out | 358 | -1 | 0.00 | 0.00 | 0.00 | 0.00 | None |
| 162B | 0.81 | 6 | 13.60 | 58.44 | 0.21 | 63.43 | AFC |

Table 20: (continued).

| Cycle | Time [d] | Neck-Shim Rods Inserted | Lobe Power [MW] | Total Power [MW] | Mod-eled Core Split[–] | Lobe Cor-rected To-tal Power [MW] | Adja-cent Loading |
|---|---|---|---|---|---|---|---|
| 162B | 10 | 6 | 22.95 | 99.53 | 0.21 | 107.05 | AFC |
| 162B | 10.73 | 5 | 23.00 | 100.76 | 0.22 | 106.81 | AFC |
| 162B-out | 2.16 | -1 | 0.00 | 0.00 | 0.00 | 0.00 | None |
| 162B | 0.09 | 5 | 4.23 | 18.18 | 0.22 | 19.64 | AFC |
| 162B | 1 | 5 | 21.08 | 92.94 | 0.22 | 97.90 | AFC |
| 162B | 11 | 5 | 22.97 | 100.44 | 0.22 | 106.67 | AFC |
| 162B | 5.34 | 3 | 22.95 | 100.43 | 0.22 | 105.07 | AFC |
| 162B-out | 73 | -1 | 0.00 | 0.00 | 0.00 | 0.00 | None |
| 164A | 0.18 | 6 | 2.46 | 10.16 | 0.21 | 11.47 | AFC |
| 164A | 1 | 6 | 12.36 | 56.78 | 0.21 | 57.65 | AFC |
| 164A | 12.24 | 6 | 22.82 | 103.81 | 0.21 | 106.43 | AFC |
| 164A-out | 9.11 | -1 | 0.00 | 0.00 | 0.00 | 0.00 | None |
| 164A | 0.64 | 6 | 12.59 | 58.34 | 0.21 | 58.72 | AFC |
| 164A | 26.51 | 6 | 22.27 | 103.16 | 0.21 | 103.86 | AFC |
| 164A-out | 2.82 | -1 | 0.00 | 0.00 | 0.00 | 0.00 | None |
| 164A | 0.67 | 6 | 16.88 | 78.52 | 0.21 | 78.73 | AFC |
| 164A | 14 | 6 | 22.29 | 102.79 | 0.21 | 103.96 | AFC |
| 164A | 0.59 | 5 | 22.12 | 101.73 | 0.22 | 102.73 | AFC |
| 164A-out | 33 | -1 | 0.00 | 0.00 | 0.00 | 0.00 | None |
| 164B | 1 | 6 | 13.65 | 63.33 | 0.21 | 63.66 | AFC |
| 164B | 25.75 | 6 | 23.00 | 104.66 | 0.21 | 107.29 | AFC |
| 164B-out | 8.26 | -1 | 0.00 | 0.00 | 0.00 | 0.00 | None |
| 164B | 0.85 | 6 | 16.12 | 73.20 | 0.21 | 75.18 | AFC |
| 164B | 10.84 | 6 | 23.15 | 103.79 | 0.21 | 107.99 | AFC |
| 164B-out | 47.53 | -1 | 0.00 | 0.00 | 0.00 | 0.00 | None |
| 164B | 0.63 | 6 | 9.89 | 44.03 | 0.21 | 46.13 | AFC |
| 164B | 12 | 6 | 23.06 | 102.22 | 0.21 | 107.53 | AFC |
| 164B | 1 | 5 | 23.10 | 99.79 | 0.22 | 107.28 | AFC |
| 164B | 11.76 | 3 | 23.16 | 101.13 | 0.22 | 106.03 | AFC |
| 164B-out | 453 | -1 | 0.00 | 0.00 | 0.00 | 0.00 | None |
| 168A | 0.94 | 6 | 11.53 | 54.28 | 0.21 | 53.77 | AFC |
| 168A | 19.82 | 6 | 22.92 | 111.01 | 0.21 | 106.90 | AFC |

Table 20: (continued).

| Cycle | Time [d] | Neck-Shim Rods Inserted | Lobe Power [MW] | Total Power [MW] | Mod-eled Core Split[–] | Lobe Cor-rected To-tal Power [MW] | Adja-cent Loading |
|---|---|---|---|---|---|---|---|
| 168A-out | 8.21 | -1 | 0.00 | 0.00 | 0.00 | 0.00 | None |
| 168A | 0.96 | 6 | 18.95 | 91.24 | 0.21 | 88.38 | AFC |
| 168A | 20.09 | 6 | 22.97 | 110.24 | 0.21 | 107.15 | AFC |
| 168A-out | 28.59 | -1 | 0.00 | 0.00 | 0.00 | 0.00 | None |
| 168A | 0.24 | 6 | 7.55 | 34.63 | 0.21 | 35.21 | AFC |
| 168A | 1 | 6 | 17.42 | 84.01 | 0.21 | 81.24 | AFC |
| 168A | 16 | 6 | 23.03 | 111.29 | 0.21 | 107.43 | AFC |
| 168A | 3.04 | 3 | 23.20 | 111.76 | 0.22 | 106.21 | AFC |
| 168A-out | 35 | -1 | 0.00 | 0.00 | 0.00 | 0.00 | None |
| 168B | 0.61 | 6 | 12.69 | 59.00 | 0.21 | 59.18 | AFC |
| 168B | 34 | 6 | 23.70 | 106.49 | 0.21 | 110.54 | AFC |
| 168B | 8.86 | 5 | 23.89 | 105.87 | 0.22 | 110.95 | AFC |
| 168B-out | 4.74 | -1 | 0.00 | 0.00 | 0.00 | 0.00 | None |
| 168B | 0.22 | 5 | 5.18 | 23.80 | 0.22 | 24.06 | AFC |
| 168B-out | 1.27 | -1 | 0.00 | 0.00 | 0.00 | 0.00 | None |
| 168B | 0.89 | 5 | 18.84 | 84.07 | 0.22 | 87.49 | AFC |
| 168B | 11.95 | 3 | 23.42 | 105.11 | 0.22 | 107.22 | AFC |
| 168B | 1.45 | 3 | 21.13 | 98.66 | 0.22 | 96.72 | AFC |
| | | | | | | | |